Supporting Information

Anja Massolle[†,‡], Thomas Dresselhaus[†,‡], Steffen Eusterwiemann[†], Carsten Doerenkamp[⊥,‖], Hellmut Eckert[1⊥,‖], Armido Studer[2†], and Johannes Neugebauer[3†,‡]

[†]Organisch-Chemisches Institut, Westfälische Wilhelms-Universität Münster, Corrensstraße 40, 48149 Münster, Germany.

[‡]Center for Multiscale Theory and Computation, Westfälische Wilhelms-Universität Münster, Corrensstraße 40, 48149 Münster, Germany.

[⊥]Institut für Physikalische Chemie, Westfälische Wilhelms-Universität Münster, Corrensstrasse 28/30, 48149 Münster, Germany.

[‖]Instituto de Física em São Carlos, Universidade de São Paulo, Avenida Trabalhador Saocarlense 400, São Carlos, SP 13566-590, Brazil.

February 26, 2018

[1]eckerth@uni-muenster.de
[2]studer@uni-muenster.de
[3]j.neugebauer@uni-muenster.de

Contents

S1   General information

¹H-NMR and **¹³C-NMR** spectra were recorded on a *Bruker DPX 300*, a *Bruker AV 300* spectrometer at room temperature. The chemical shifts were referred to the solvent residual peak (CDCl$_3$: ¹H: δ7.26 ppm, ¹³C: δ77.16 ppm; DMSO-d$_6$: ¹H: δ2.50 ppm, ¹³C: δ39.52 ppm). Multiplicities of NMR signals are described as s (singlet), d (doublet), t (triplet), m (multiplet) or br (broad signal). **Mass spectra** (HRMSESI) were recorded on a *Finnigan* MAT 4200S, *Bruker* Daltonics Micro-TOF, a *Micromass* Quatro LCZ (ESI) or a *Bruker* LTQ Orbitrap XL and peaks are given in molar mass to charge ratios m/z. **IR spectra** were recorded on a *Digilab* Varian 3100 FT-IR Excalibur Series equipped with a MKII Golden Gate Single Reflection ATR unit. Recorded IR signals are reported in wavenumber (cm^{-1}) with the following abbreviation for the intensity of absorption: s = strong, m = medium, w = weak. **Melting points** (M.p.) were measured on a *Stuart* SMP-10 and a *Stuart* SMP3 melting point apparatus and are uncorrected. **Thin layer chromatography** (TLC) was carried out on **Merck** silica gel 60 F254 plates; detection by UV (irradiation at 254 nm) or dipping into a solution of KMnO$_4$ (1.5 g), NaHCO$_3$ (5.0 g) in H$_2$O (400 mL), followed by heating. **Flash chromatography** (FC) was performed on silica gel (*Merck*-Si 60: $40 - 63$ µm) with a pressure of 0.1 to 0.5 bar. Used eluents are given in parentheses. **Solvents:** All solvents for extraction and FC were distilled before use. Et$_2$O was distilled from K/Na and CH$_2$Cl$_2$ was distilled from P$_2$O$_5$ under argon atmosphere before use.

Techniques: All reactions involving air or moisture sensitive reagents or intermediates were carried out under argon atmosphere using standard *Schlenk* techniques. All glasswares were dried by the use of a heat gun under high vacuum prior to use. Concentration of the reaction mixture was performed under reduced pressure at 40 °C at the appropriate pressure. Purified compounds were further dried under high vacuum. All **reagents** were purchased of the following companies and have been used with-

out further purification: *Acros Organics*, *Sigma-Aldrich*, *Alfa Aesar*, *TCI Germany* or *Merck*. Iodobenzene-d$_5$, 2,4-diphenylcarbonohydrazide (**1a**), 1,5-diphenyl-3-tert-butyl-6-oxo-verdazyl (**3a**), 1,5-diphenyl-3-mesityl-6-oxo-verdazyl (**3c**), 1,5-diphenyl-3-(naphthalen-1-yl)-6-oxo-verdazyl (**3g**), 1,5-diphenyl-3-(anthracen-9-yl)-6-oxo-verdazyl (**3h**), 1,5-diphenyl-3-(pyren-1-yl)-6-oxo-verdazyl (**3i**) and 6-trimethylsilylethinyl-2,4-diphenyl-3-oxo-verdazyl (**3k**) were synthesized in accordance to literature procedures [1–3].

S2 Experimental procedures

S2.1 General procedures
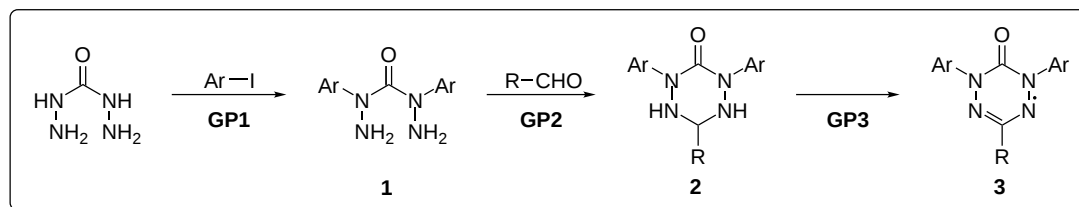
Scheme S-1: Synthesis of verdazyl radicals **3**.

GP1: Synthesis of diaryl substituted carbonohydrazides (1)

According to a literature procedure described by *Masuda et al.* [4] CuI (5.0 mol%), 1,10-phenanthroline (10 mol%), K_3PO_4 (3.1 eq.) and carbohydrazide (1.0 eq.) were added. Aryl iodide $(2.2 - 2.3$ equiv.) and DMF (2.0 mL/mmol carbohydrazide) were added and the mixture was stirred at 90 °C. Afterwards the reaction mixture was cooled to rt and filtered through a short pad of silica and washed with EtOAc. H_2O was added and the two layers were separated. The aqueous layer was extracted twice with EtOAc and the combined organic layers were washed with brine and dried over $MgSO_4$. Filtration, removal of the solvent *in vacuo* and FC afforded the appropriate diaryl substituted carbonohydrazides.

GP2: Synthesis of tetrazinan-3-ones (2)

In a two-necked flask with condenser carbonohydrazide (1.0 eq.) was dissolved in MeOH and stirred at 40 °C for 5 min. A solution of an aldehyde (1.0 eq.) in MeOH (4 mL/mmol) was added dropwise within 30 min. After addition the mixture was refluxed for $3 - 4$ h. The reaction mixture was cooled to rt, the precipitate was filtered off and washed carefully with cold MeOH. The solid was dried *in vacuo* to afford the tetrazinan-3-one.

GP3: Synthesis of verdazyl Radicals (3)

In a sealed tube tetrazinan-3-one (1.0 eq.) and 1,4-benzoquinone (1.7 eq.) were dissolved in CH_2Cl_2 (10 mL/mmol). The reaction mixture was stirred at 60 °C for $3-4$ h. After cooling to rt, the reaction mixture was filtered and the solvent was removed *in vacuo*. FC afforded the verdazyl radical as a solid.

S2.2 Synthesis of carbonohydrazides

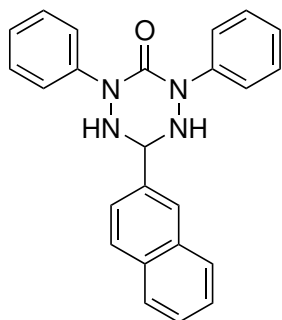**2,4-Di-d$_5$-phenylcarbonohydrazide (1b)**

According to **GP1** with carbohydrazide (229 mg, 2.55 mmol, 1.0 eq.), iodobenzene-d$_5$ (1.20 g, 5.74 mmol, 2.25 eq.), CuI (24 mg, 0.13 mmol, 5.0 mol%), 1,10-phenanthroline (55 mg, 0.26 mmol, 10 mol%) and K_3PO_4 (1.65 g, 7.78 mmol, 3.1 eq.) in DMF (5 mL) at 90 °C for 40 h. FC (*n*-pentane/MTBE 4:1) afforded **1b** (404 mg, 1.60 mmol, 63%) as a yellow solid.

$C_{13}H_4D_{10}N_4O$
252.34 g/mol

M.p.: 70 °C; **IR** (ATR, neat): 3334w, 3204w, 2272w, 1649s, 15559s, 1366s, 1308s, 1204m, 1077w, 1037w, 912m, 816m, 745w, 675w, 628w; **^{1}H-NMR** (300 MHz, CDCl$_3$): $\delta 4.21$ (br s, 4H, NH$_2$); **^{13}C-NMR** (75 MHz, CDCl$_3$): $\delta 161.9$ (C), 144.6 (C), 128.4 (t, $J = 24.3$ Hz, CD), 124.9 (t, $J = 24.3$ Hz, CD), 123.3 (t, $J = 24.3$ Hz, CD); **HRMS** (ESI): $m/z = $ 253.1868 calcd. for $[M+H]^+$, found: 253.1860.

S2.3   Synthesis of differently substituted tetrazinan-3-ones

**6-(Naphthalen-2-yl)-2,4-diphenyl-1,2,4,5-tetrazinan-3-one (2e)**

According to **GP2** with 2,4-diphenylcarbonohydrazide (121 mg, 500 µmol, 1.0 eq.) and 2-naphthaldehyde (78 mg, 0.50 mmol, 1.0 eq.). Filtration afforded the title compound (131 mg, 350 µmol, 69%) as a colorless solid.

C$_{24}$H$_{20}$N$_4$O
380.44 g/mol

M.p.: 216 °C; **IR** (ATR, neat): 3330w, 3237m, 3056w, 1674w, 1623m, 1595m, 1491m, 1453m, 1366s, 1307s, 1220w, 1180w, 1134w, 1116w, 1076w, 1029w, 980w, 918s, 882m, 859s, 833m, 815s, 796m, 747s, 729s, 708w, 692s, 670m, 641m, 622w, 569m, 548m, 530w, 505s; **^{1}H-NMR** (300 MHz, DMSO-d$_6$): δ8.08 (s, 1H, CH$_{arom}$), 7.91 (d, J = 8.8 Hz, 2H, CH$_{arom}$), 7.84 (dd, J = 6.1, 3.4 Hz, 1H, CH$_{arom}$), 7.71 (d, J = 1.6 Hz, 1H, CH$_{arom}$), 7.68 – 7.64 (m, 4H, CH$_{arom}$), 7.53 (dt, J = 6.2, 3.4 Hz, 2H, CH$_{arom}$), 7.40 – 7.30 (m, 4H, CH$_{arom}$), 7.10 (t, J = 7.3 Hz, 2H, CH$_{arom}$), 6.52 (d, J = 9.0 Hz, 2H, NH), 5.58 (t, J = 9.0 Hz, 1H, CH); **^{13}C-NMR** (101 MHz, DMSO-d$_6$): δ156.6 (C), 142.8 (C), 135.0 (C), 132.6 (C), 132.5 (C), 127.9 (CH), 127.8 (CH), 127.8 (CH), 127.4 (CH), 126.2 (CH), 126.1 (CH), 125.8 (CH), 124.9 (CH), 123.2 (CH), 121.2 (CH), 72.8 (CH); **HRMS** (ESI): m/z = 403.1529 calcd. for [M+Na]$^+$, found: 403.1534.

S2.4   Synthesis of verdazyl radicals

**1,5-Di(d$_5$-phenyl)-3-tert-butyl-6-oxo-verdazyl radical (3b)**
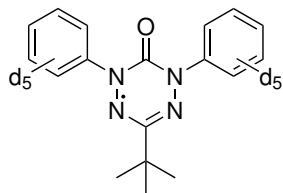
C$_{18}$H$_9$D$_{10}$N$_4$O
317.43 g/mol

A solution of pivalaldehyde (20 µL, 0.18 mmol, 1.0 eq.) in MeOH (1 mL) was added to a solution of 2,4-di-d$_5$-phenylcarbonohydrazide (46 mg, 0.18 mmol, 1.0 eq.) in MeOH (1 mL) at 40 °C within 20 min. The reaction mixture was stirred at 60 °C for 3 h. Filtration of the reaction mixture afforded a colorless solid, which was washed with cold Et$_2$O and dried *in vacuo* to afford the tetrazinan-3-one (28 mg, 90 µmol, 49%) as a colorless solid. According to **GP3** the solid was directly reacted with 1,4-benzoquinone (16 mg, 0.15 mmol, 1.7 eq.) in CH$_2$Cl$_2$ (4.5 mL) at 60°C for 3 h. FC (n-pentane/acetone 10:1) afforded verdazyl radical **3b** (9 mg, 0.03 mmol, 31%) as a black solid.

M.p.: 116 °C; **IR** (ATR, neat): 1694s, 1556w, 1480w, 1372s, 1293w, 1251m, 1206w, 1166s, 1025w, 905w, 822w, 745w, 635w; **HRMS** (ESI): $m/z = 340.2079$ calcd. for [M+Na]$^+$, found: 340.2088.

1,5-Di(d$_5$-phenyl)-3-mesityl-6-oxo-verdazyl (3d)
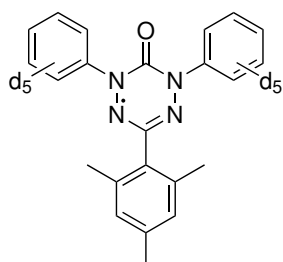
C$_{23}$H$_{11}$D$_{10}$N$_4$O
379.50 g/mol

A solution of 2,4,6-trimethylbenzaldehyd (24 µL, 0.16 mmol, 1.0 eq.) in MeOH (1 mL) was added to a solution of 2,4-di-d$_5$-phenylcarbonohydrazide (40 mg, 0.16 mmol, 1.0 eq.) in MeOH (1 mL) at 40 °C within 20 min. The reaction mixture was stirred at 60 °C for 3 h. Filtration of the reaction mixture afforded a colorless solid, which was washed with cold Et$_2$O and dried *in vacuo* to afford the tetrazinan-3-one (26 mg, 70 µmol, 41%). According to **GP3** the solid was reacted with 1,4-benzoquinone (12 mg, 0.12 mmol, 1.7 eq.) in CH$_2$Cl$_2$ (4.5 mL) at 60 °C for 3 h. FC (n-pentane/MTBE 10:1) afforded verdazyl radical

3d (9 mg, 0.02 mmol, 36%) as a black solid.

M.p.: 146 °C; **IR** (ATR, neat): 1705s, 1610w, 1559w, 1445m, 1373s, 1295w, 1223s, 1167m, 1107m, 1030m, 961w, 847m, 768w, 716w; **HRMS** (ESI): $m/z = 402.2235$ calcd. for $[M+Na]^+$, found: 402.2241.

1,5-Diphenyl-3-(2-naphthyl)-6-oxo-verdazyl (3e)
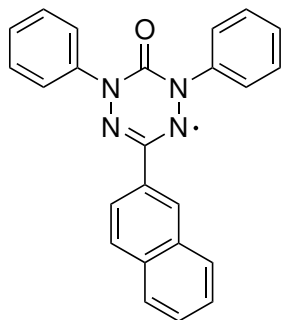
C$_{24}$H$_{17}$N$_4$O
377.42 g/mol

According to **GP3** with 6-(naphthalen-2-yl)-2,4-diphenyl-1,2,4,5-tetrazinan-3-one (0.33 g, 0.85 mmol, 1.0 eq.) and 1,4-benzoquinone (0.36 g, 3.4 mmol, 3.9 eq). FC (n-pentane/CH$_2$Cl$_2$ 5:1) afforded verdazyl radical **3e** (0.31 g, 0.83 mmol, 96%) as a dark red solid.

M.p.: 212 °C. **IR** (ATR, neat): 3058w, 2921w, 2853w, 1770m, 1721m, 1685s, 1595m, 1488s, 1456m, 1488s, 1335s, 1305s, 1227m, 1165s, 1131m, 1111m, 1073m, 1036m, 993w, 865w, 822m, 752s, 734s, 695s, 654m, 604m, 588m, 558m; **HRMS** (ESI): $m/z = 400.1295$ calcd. for $[M+Na]^+$, found: 400.1300.

1,5-Di(d$_5$-phenyl)-3-(2-naphthyl)-6-oxo-verdazyl (3f)
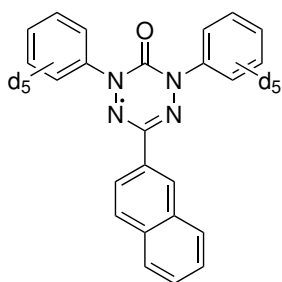
C$_{24}$H$_7$D$_{10}$N$_4$O
387.48 g/mol

A solution of 2-naphthaldehyde (35 mg, 0.23 mmol, 1.0 eq.) in MeOH (1 mL) was added to a solution of 2,4-di-d$_5$-phenylcarbonohydrazide (57 mg, 0.23 mmol, 1.0 eq.) in MeOH (1 mL) at 40 °C within 20 min. The reaction mixture was stirred at 60 °C for 3 h. Filtration of the reaction mixture afforded a colorless solid, which was washed with cold Et$_2$O and dried in vacuo to afford the tetrazinan-3-one (42 mg, 0.11 mmol, 46%). According to **GP3** the solid was reacted with 1,4-benzoquinone (20 mg, 0.19 mmol, 1.7 eq.) in CH$_2$Cl$_2$ (4.5 mL) at 60 °C for 3 h. FC (n-pentane/MTBE 8:1) afforded verdazyl radical

3f (24 mg, 0.06 mmol, 56%) as a dark solid.

M.p.: 218 °C; **IR** (ATR, neat): 2829w, 1682s, 1596w, 1509w, 1460m, 1380m, 1343m, 1165m, 1141w, 1021w, 963w, 871m, 834m, 747s, 629w; **HRMS** (ESI): $m/z = 410.1922$ calcd. for $[M+Na]^+$, found: 410.1937.

S3 Solvent Effects on EPR-Spectra

For some of the experiments, the solvent for the EPR measurements was changed from toluene to dichloromethane (CH_2Cl_2) (see Tab. II in the main text). To investigate the influence of this change, we discuss in the following the consequences of the solvent on the measured spectrum and the results of the quantum chemical calculations.

Fig. S1 depicts the experimental spectrum of radical **3a** measured in toluene and CH_2Cl_2. The shape of the spectra differs and the spectrum measured in CH_2Cl_2 seems to be more resolved. However, broadening the peaks of the spectrum measured in CH_2Cl_2 would not lead to the spectrum measured in toluene since a lot of peak positions are slightly different. Moreover, the peak pattern around a *g*-factor of 2.013 to 2.008 and 2.002 to 1.996 differs between the solvents.
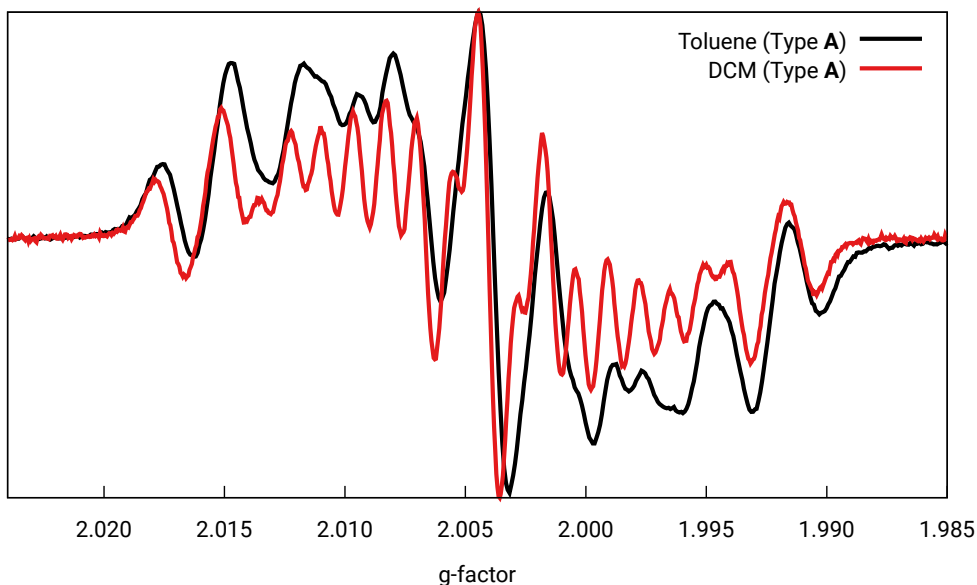
Figure S1: Experimental spectrum of compound **3a** measured in toluene (modulation amplitude: 0.6G) and CH_2Cl_2 (modulation amplitude: 0.3G).

The MD QM calculated (type **C**) and fitted (type **D**) EPR parameters for compound **3a** dissolved in toluene and CH_2Cl_2 are listed in Tab. S1. In the MD QM calculations the changes in the ^{14}N hyperfine coupling constants are 0.24 MHz at most. For the ^{1}H nuclei

the maximum change is around 0.1 MHz. Considering the fitted results the deviations are somewhat more pronounced, though of the same order of magnitude. Here, the largest change is 0.32 MHz for the ^{14}N HFCCs and 0.36 MHz for the ^{1}H nuclei.

This could be caused by the fact that an implicit solvent model does not capture all solvent effects. Nevertheless, several publications [5–9] showed that an implicit solvent model is adequate for the calculation of EPR parameters and, regarding the results of the other investigated compounds, we also achieved good agreement with the experimental data by using an implicit solvent model.

From these tests we can conclude that the solvent effect on the calculated EPR parameters are tiny while the shape of the experimental spectrum of **3a** changes more significantly when changing the solvent. During the fitting procedure the HFCCs of the ^{1}H nuclei mimic these changes to a certain extent.

Table S1: MD QM (type **C**) calculated and fitted (type **D**) EPR parameters of radical **3a** dissolved in CH_2Cl_2 and toluene.

System		g-shift	$A_{N1,5}$ MHz	$A_{N2,4}$ MHz	$A_{H, ortho}$ MHz	$A_{H, meta}$ MHz	$A_{H, para}$ MHz
			CH_2Cl_2				
3a	MD QM	0.0017	13.024	17.939	−1.944	1.491	−1.712
	Fit	0.0017	12.425	18.472	−1.533	1.081	−1.575
			Toluene				
3a	MD QM	0.0018	12.648	17.817	−2.033	1.497	−1.818
	Fit	0.0015	12.373	18.190	−1.964	1.433	−1.694

S4   Molecular Dynamics

In the following we present more details about the validation of the computational protocol.

S4.1 Thermal Situation of the Systems

Translational and rotational velocity contributions are removed during the NVT simulations, which are used to heat up the system. Therefore, the initial velocities for the NVE production run are free from translational and rotational movements. In the following we check whether tanslational and rotational velocities are build up in the NVE MD.

In Tab. S2 the average temperatures of the NVE MD production runs are listed. They vary between 298 and 300 K, which indicates that all systems were treated equally. Furthermore, we removed translational and rotational velocity components and revaluate the temperature at every MD step during an NVE run. Figure S2 depicts the temperature with and without translational and rotational velocity components at every MD step. The results are within numerical accuracy. From this we can conclude that no rotation and translation is building up during the NVE simulation.

Table S2: Average temperature in the NVE MD runs for the spectra shown in Figs. 6 and 7.

System	average temperature / K
3a	299
3c	299
3e	298
3g	299
3h	299
3i	298
3j	299
3k	300
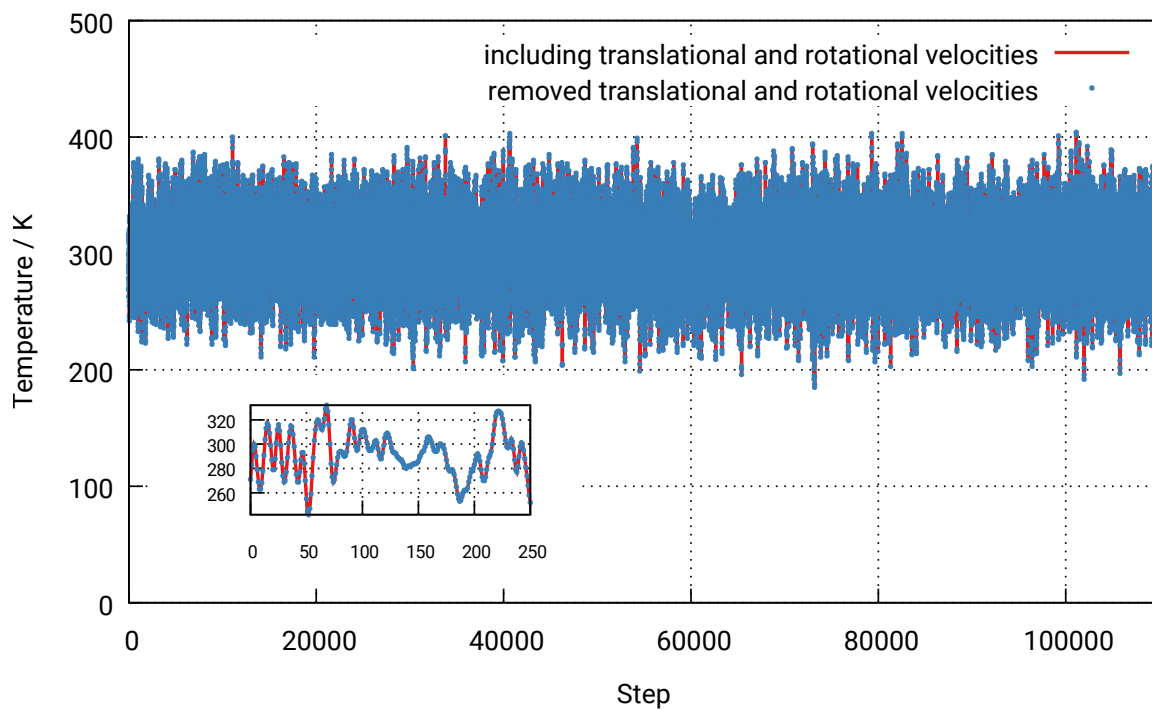
Figure S2: Temperature per time step in a NVE MD simulation for **3a**.

S4.2 Convergence of HFCCs

Tab. S3 lists the average HFCC values and corresponding standard deviations for three different trajectories of system **3a** with different sampling times and sampling frequencies. The large standard deviation clearly shows the sensitivity of the HFCC values on changes in the geometry.

Table S3: HFCC values and standard deviations for three different trajectories of **3a**, dissolved in toluene, with different sampling times and sampling frequencies. The listed values correspond to the N1, N2, N4 and N5 nitrogen.

| t_s	ν_s	#	Trj.	HFCC value MHz				Standard deviation MHz			
ps	ps^{-1}	geom.		A_{N1}	A_{N5}	A_{N2}	A_{N4}	σ_{N1}	σ_{N5}	σ_{N2}	σ_{N4}
50	2.0	100	1	12.77	12.52	17.99	17.64	3.33	3.54	1.97	2.06
			2	12.96	12.00	18.39	16.61	3.88	3.06	1.99	1.75
			3	12.02	11.34	17.63	16.92	2.81	2.71	1.76	1.91
50	0.4	20	1	13.28	12.21	18.54	17.57	3.34	3.09	1.93	2.16
			2	14.43	12.07	18.51	16.40	4.97	3.46	2.34	1.37
			3	11.89	11.79	17.54	17.26	2.96	3.31	1.95	2.08
50	0.2	10	1	11.67	13.25	18.64	18.27	2.66	3.78	1.30	1.96
			2	13.60	12.47	18.19	16.30	3.59	4.52	2.36	1.20
			3	11.55	12.08	17.34	17.47	2.83	3.75	1.89	2.08
50	0.1	5	1	11.26	14.24	18.71	17.86	3.49	4.16	1.44	1.44
			2	12.67	10.27	19.81	15.66	1.83	1.70	1.82	1.10
			3	9.53	14.86	16.32	18.69	0.95	3.36	0.95	1.43
500	0.4	200	1	12.78	11.87	17.67	17.13	3.56	2.96	1.93	2.07
			2	12.07	11.92	17.47	17.20	3.21	2.89	2.01	1.91
			3	12.31	12.01	17.53	17.36	3.59	3.25	2.16	2.32
500	0.2	100	1	12.89	12.21	17.44	17.27	3.79	3.16	1.86	2.06
			2	12.20	11.90	17.65	17.23	3.29	3.06	1.88	1.74
			3	12.35	12.02	17.54	17.44	3.45	3.16	2.10	2.35
500	0.1	50	1	13.41	11.83	17.90	16.94	3.83	3.04	1.86	1.99
			2	12.23	11.69	17.92	17.13	2.71	3.22	1.83	1.83
			3	12.64	11.66	17.82	17.08	3.26	2.50	2.14	2.02
SP[a]	—	—	—	9.93	10.68	15.28	17.30	—	—	—	—

[a] SP = single point calculation on the optimised structure.

Also the convergence of ^{14}N and ^{1}H coupling constants for different sampling times and sampling frequencies is shown.
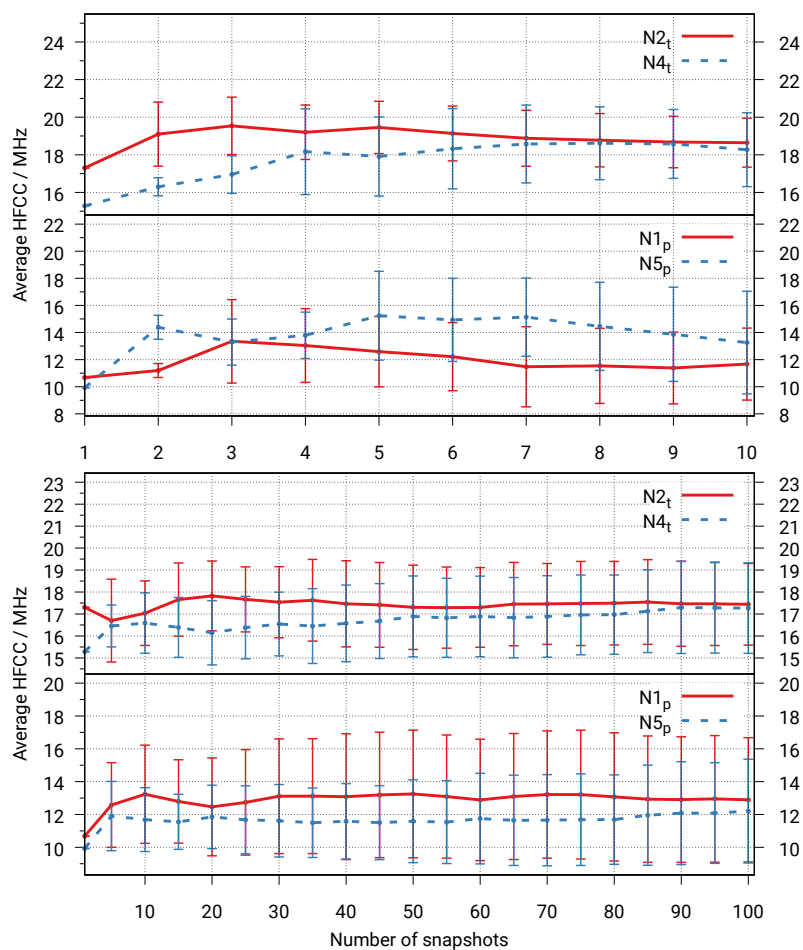
Figure S3: Average ^{14}N HFCC values and standard deviations of compound **3a** as a function of the number of geometries included in the average. The snapshots are taken from the second trajectory with a simulation time of top: 50 ps and bottom: 500 ps. The sampling frequency was 0.2 ps^{-1} for the trajectory for both simulation times. Nitrogen atoms which are connected to the phenyl groups are denoted with an index "p" and those which are in the neighborhood to the *tert*-butyl group with an index "t".
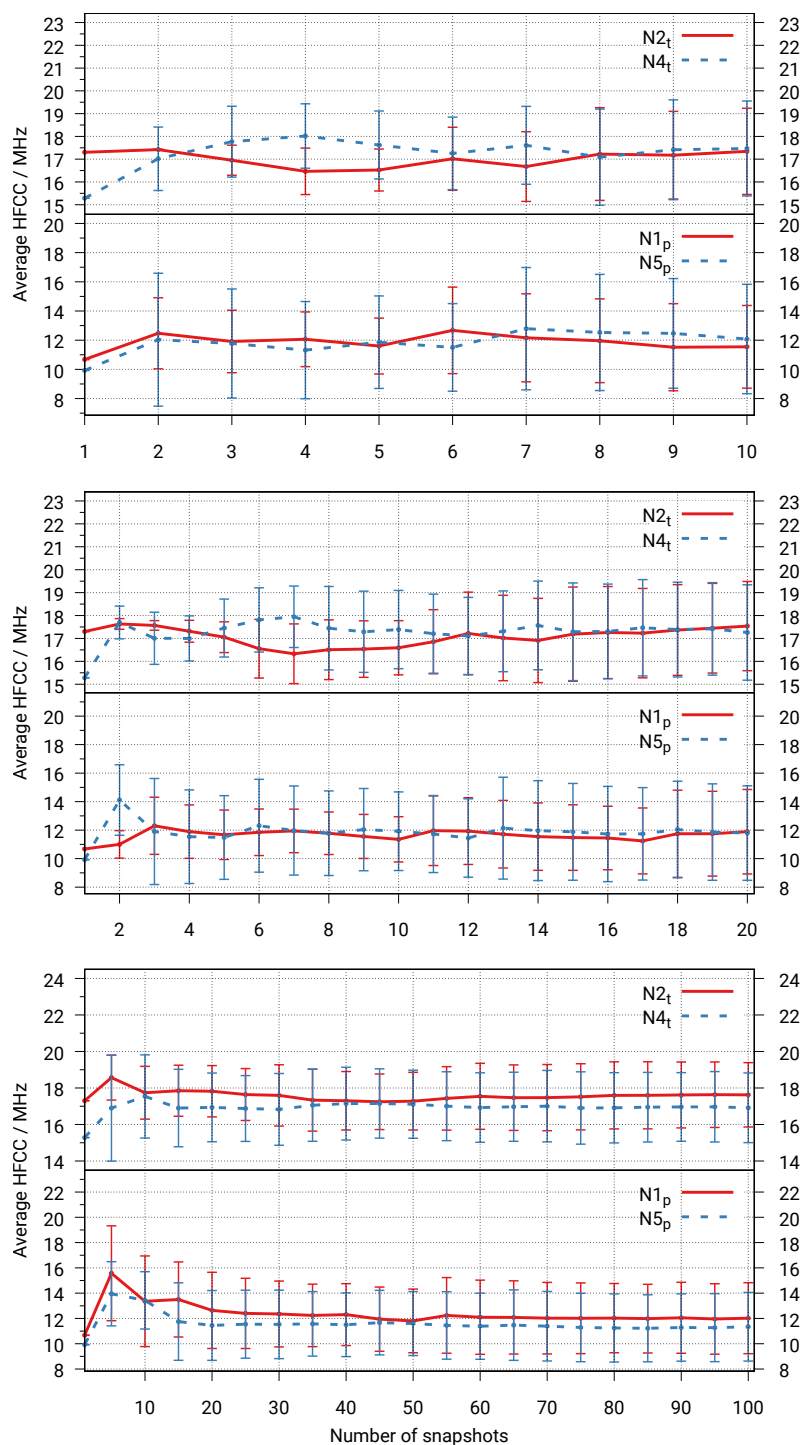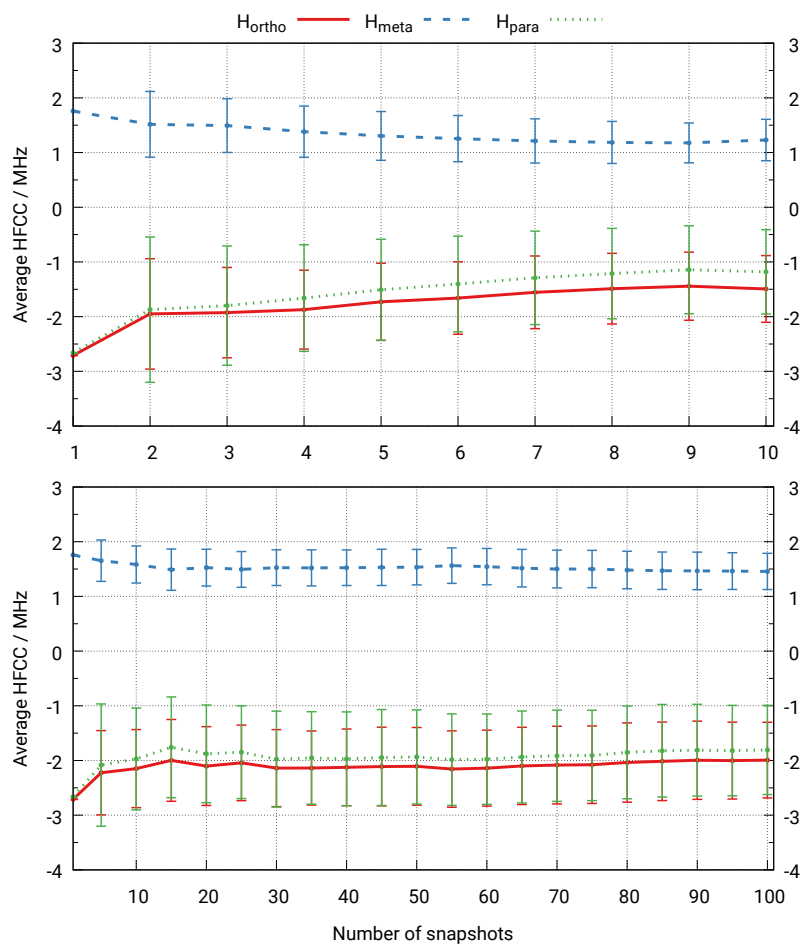
Figure S4: Average ^{14}N HFCC values and standard deviations of compound **3a** as a function of the number of geometries included in the average. The snapshots are taken from a trajectory with a simulation time of 50 ps and a constant sampling frequency of 0.2 ps^{-1} (top), 0.4 ps^{-1} (center) and 2.0 ps^{-1} (bottom), respectively. Nitrogen atoms which are connected to the phenyl groups are denoted with an index "p" and those which are in the neighborhood to the *tert*-butyl group with an index "t".
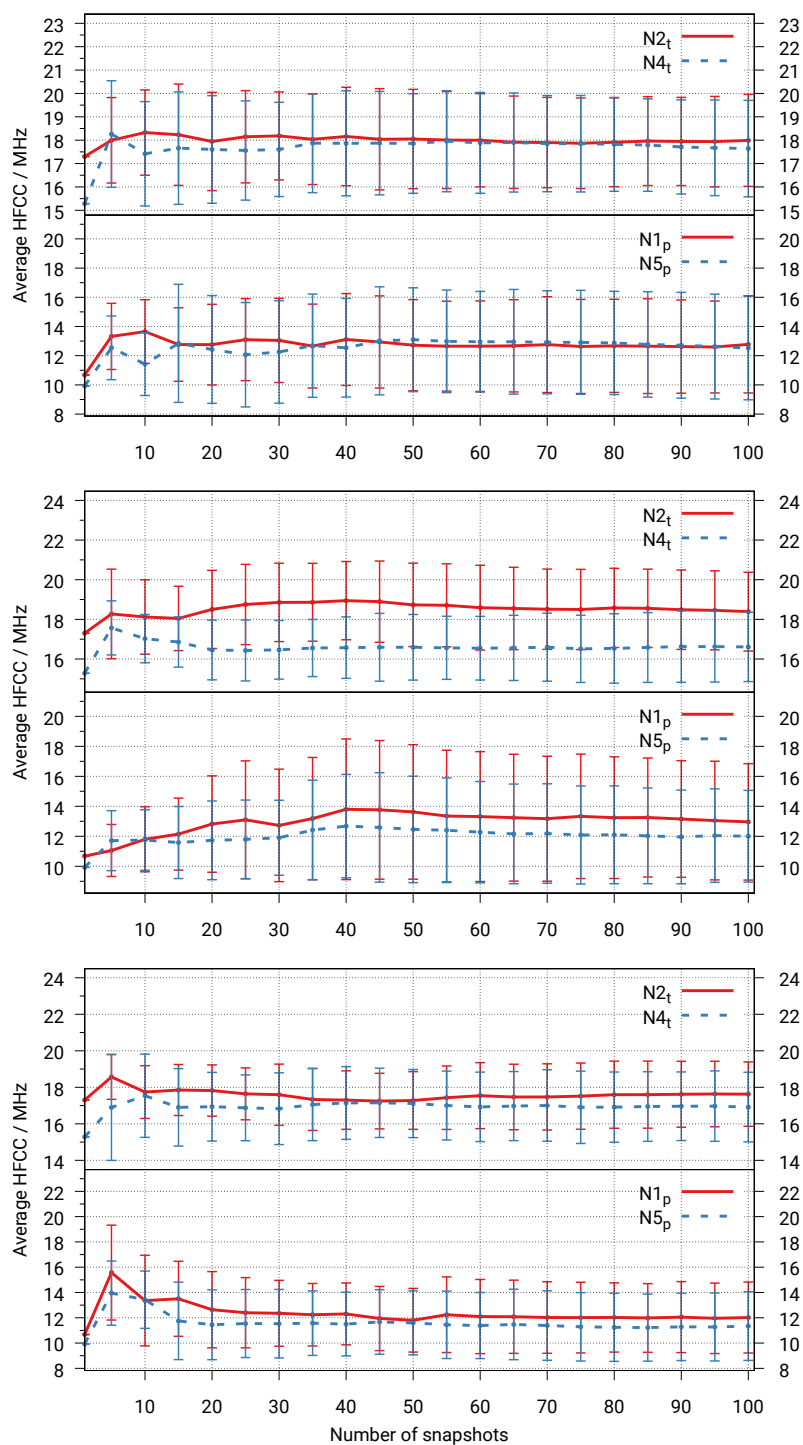
Figure S5: Average ^{14}N HFCC values and standard deviations of compound **3a** as a function of the number of geometries included in the average. The snapshots are taken from three different trajectories with a simulation time of 50 ps and a sampling frequency of 2.0 ps^{-1}. Nitrogen atoms which are connected to the phenyl groups are denoted with an index "p" and those which are in the neighborhood to the *tert*-butyl group with an index "t".
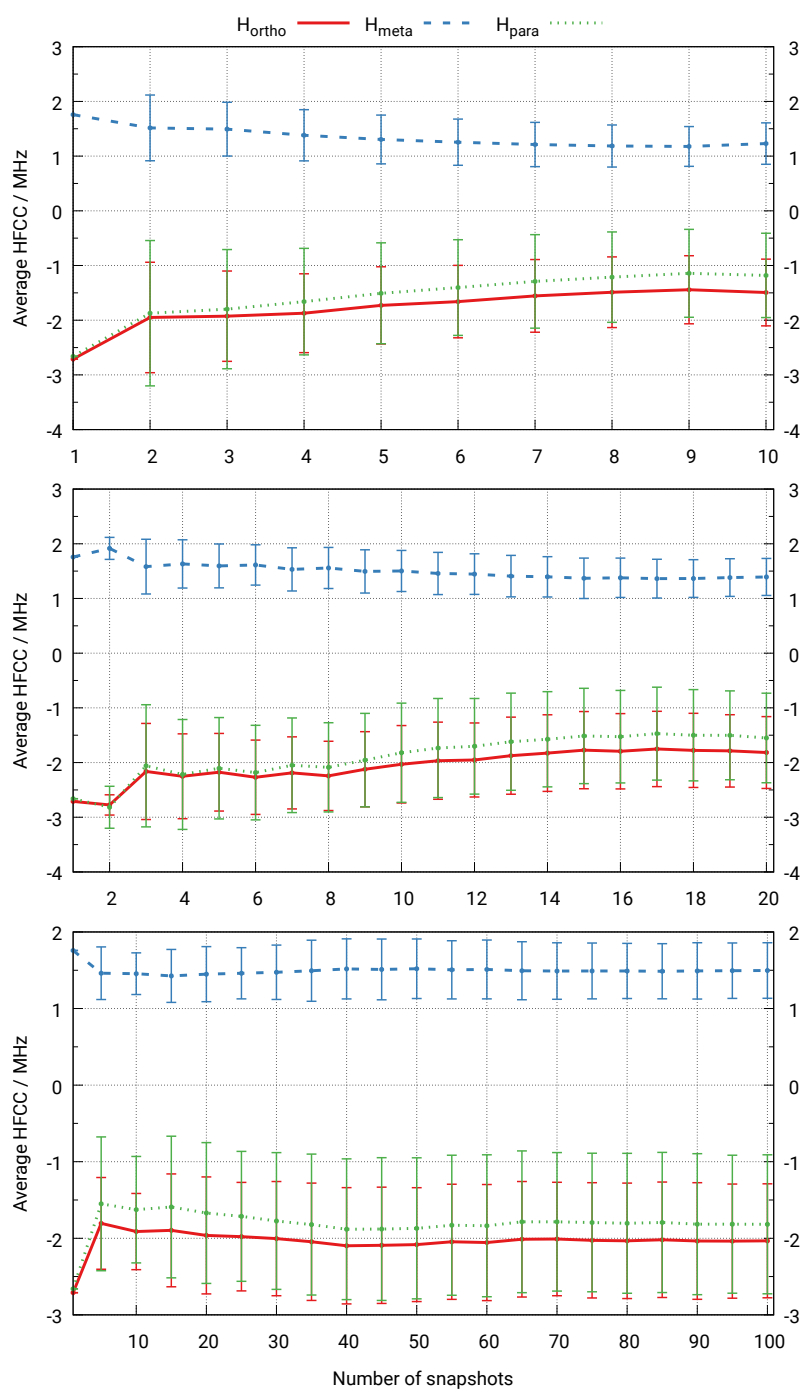
Figure S6: Average ^{1}H HFCC values and standard deviations of compound **3a** as a function of the number of geometries included in the average. The snapshots are taken from a trajectory with a simulation time of top: 50 ps and bottom: 500 ps. The sampling frequency was 0.2 ps^{-1} for the trajectory for both simulation times.
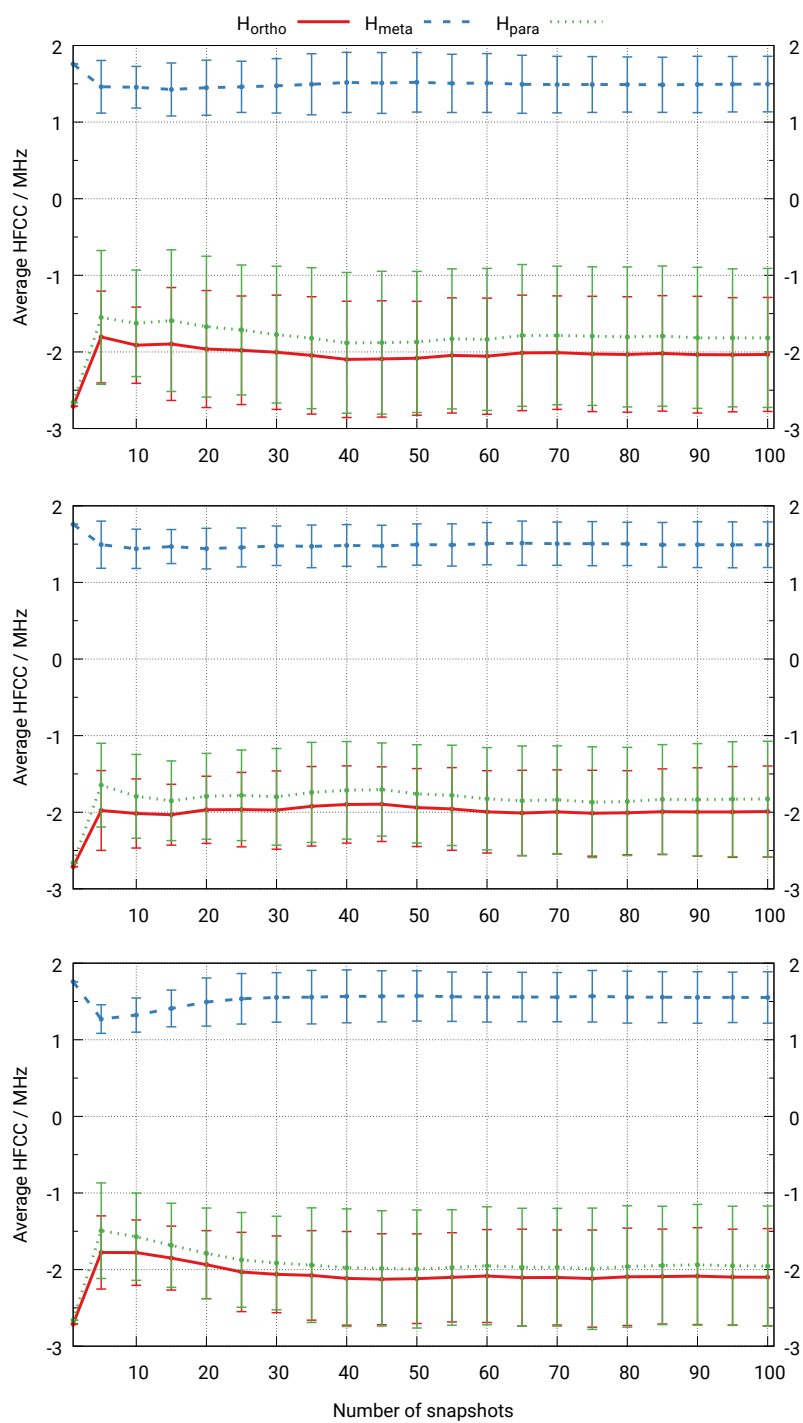
Figure S7: Average ^{1}H HFCC values and standard deviations of compound **3a** as a function of the number of geometries included in the average. The snapshots are taken from a trajectory with a simulation time of 50 ps and a constant sampling frequency of 0.2 ps^{-1} (top), 0.4 ps^{-1} (center) and 2.0 ps^{-1} (bottom), respectively.

Figure S8: Average ^{1}H HFCC values and standard deviations of compound **3a** as a function of the number of geometries included in the average. The snapshots are taken from three different trajectories with a simulation time of 50 ps and a sampling frequency of 2.0 ps^{-1}.

S4.3   Autocorrelation Functions

Here, we present the autocorrelation functions of the ^{14}N and ^{1}H HFCC values of radical **3a** for different simulation times. The autocorrelation function R_h was calculated as

$$R_h = \frac{C_h}{C_0} \tag{S1}$$

$$C_h = \frac{1}{N} \sum_{t=1}^{N-h} (y_t - \bar{y})(y_{t+h} - \bar{y}), \tag{S2}$$

with h being the lag between the snapshots, N the number of snapshots, y the value of the HFCC for the snapshot taken at this time point and $\bar{y}$ the mean average of the HFCCs. To plot the autocorrelation function with respect to the time lag, h is multiplied with the time interval between the snapshots. The autocorrelations R_h are calculated for $h = 0, 1, \ldots, H$, where H is not larger than $N/4$.

The estimated standard error (SE) for the autocorrelation function at lag h was calculated as

$$SE(R_h) = \sqrt{\frac{1}{N}\left(1 + 2\sum_{i=1}^{q} R_i^2\right)} \qquad h > q. \tag{S3}$$
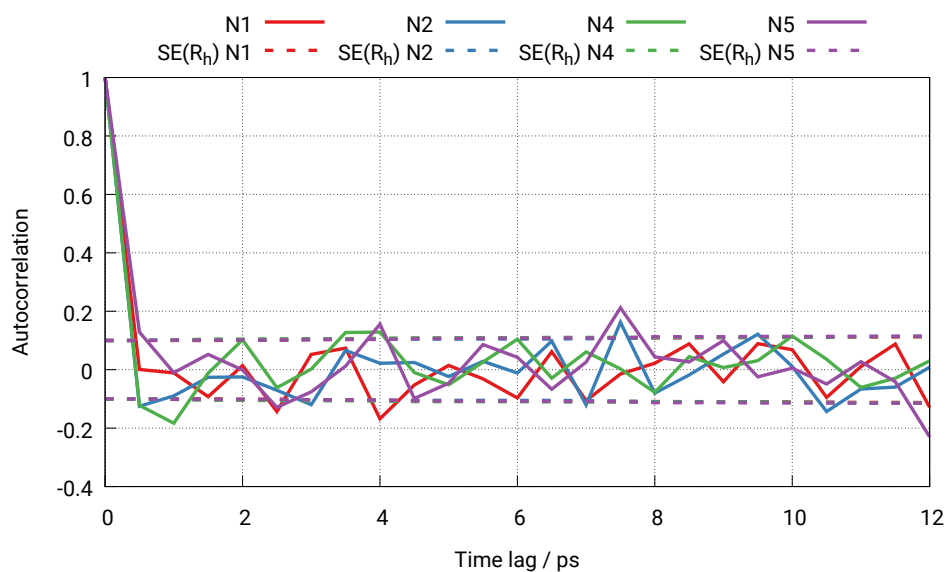
Figure S9: Autocorrelation functions for the HFCC values of the ^{14}N nuclei of system **3a** with a simulation time of 50 ps and a sampling frequency of 2.00 ps^{-1}.
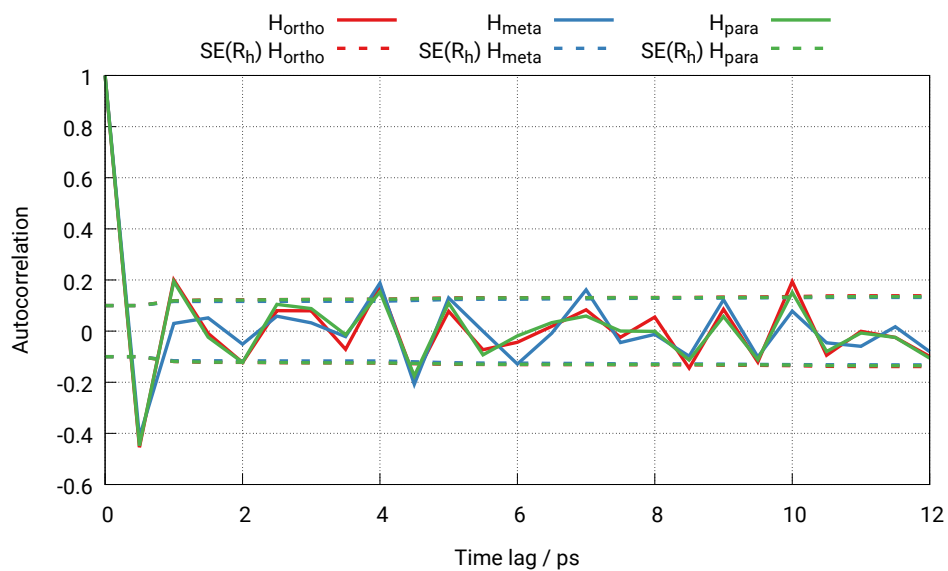
Figure S10: Autocorrelation functions for the HFCC values of the ^{1}H nuclei of system **3a** with a simulation time of 50 ps and a sampling frequency of 2.00 ps^{-1}.
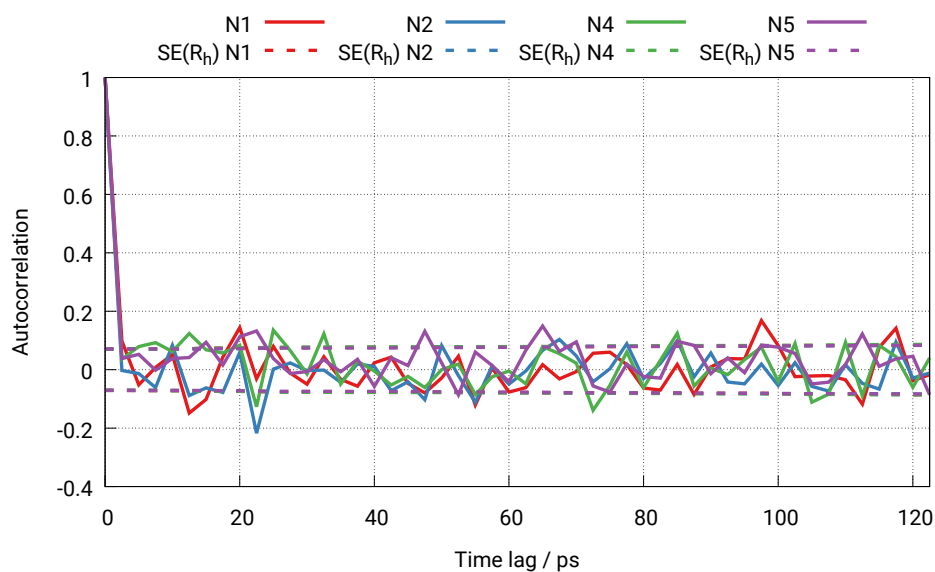
Figure S11: Autocorrelation functions for the HFCC values of the ^{14}N nuclei of system **3a** with a simulation time of 500 ps and a sampling frequency of 0.40 ps^{-1}.

Figure S12: Autocorrelation functions for the HFCC values of the ^{1}H nuclei of system **3a** with a simulation time of 500 ps and a sampling frequency of 0.40 ps^{-1}.

We observe oscillations of the autocorrelation functions which are of the order of magnitude of the standard error already for the shortest time lags. In particular the important ^{14}N HFCCs appear to be uncorrelated already for very short times, thus justifying our sampling frequency of 2.00 ps^{-1}. Only the $^{1}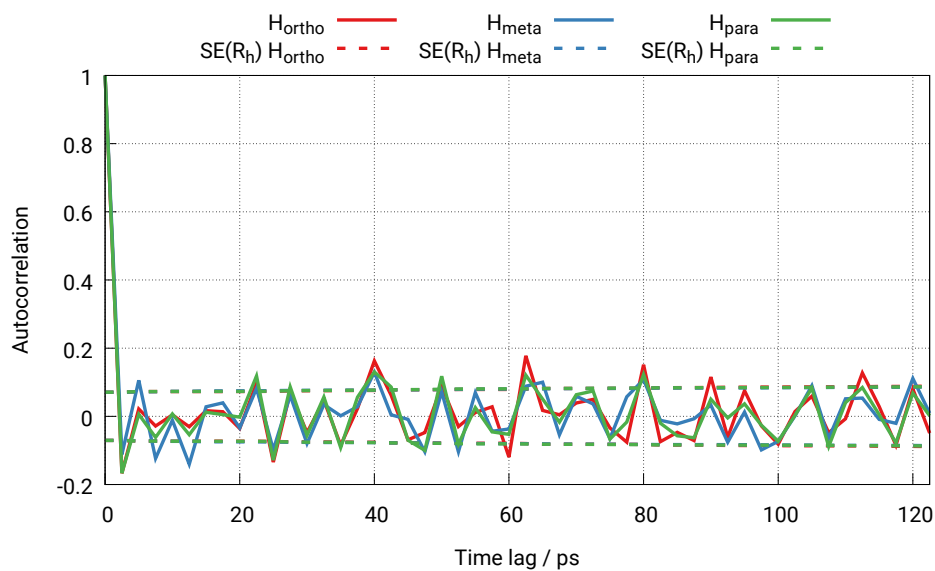$H-HFCC autocorrelations in Fig. S10 could indicate a weak correlation for time lags of 0.5-1 ps, thus effectively reducing the number of independent data points in our sampling by a factor of ~ 2. In view of the fact that the average values are nicely converged (see Fig. S8) and actually very similar to the average HFCCs obtained with longer time lags between the snapshots, our sampling setup can be considered reasonable also for these cases.

The autocorrelation functions for the *ortho*, *meta* and *para* hydrogen atoms are very similar. This is caused by the fact that the HFCCs of the different hydrogen species are strongly correlated (see Fig. S13). The reason for this is that the dihedral angle which describes the rotation of the phenyl group with respect to the verdazyl ring is strongly correlated with the HFCC values of the hydrogen atoms at the phenyl groups (this is shown in Fig. S14). If the phenyl group stands perpendicular to the verdazyl ring the absolute HFCC value is very low since the conjugated π system can not be delocalized to the phenyl substituents. Likewise, the absolute HFCCs of the hydrogen atoms at the phenyl group are large if the phenyl group is parallel orientated to the verdazyl ring. From this it follows that the HFCCs of all hydrogen atoms at the phenyl groups are correlated with the dihedral angle of the phenyl group with respect to the verdazyl ring and therefore, they are also correlated with each other.
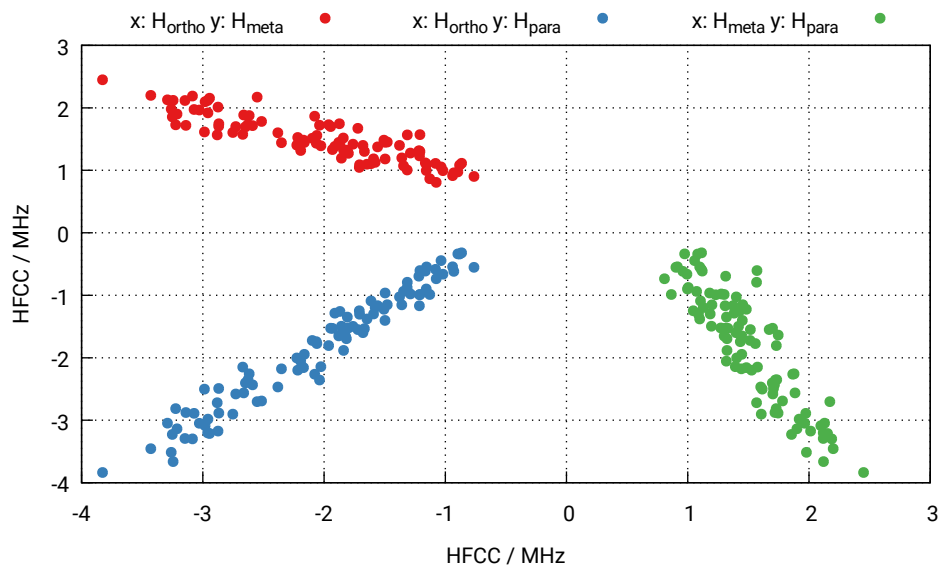
Figure S13: Correlation plot of the HFCC values of the different hydrogen species located at the phenyl groups. The HFCC values are averaged over all atoms of the observed species.
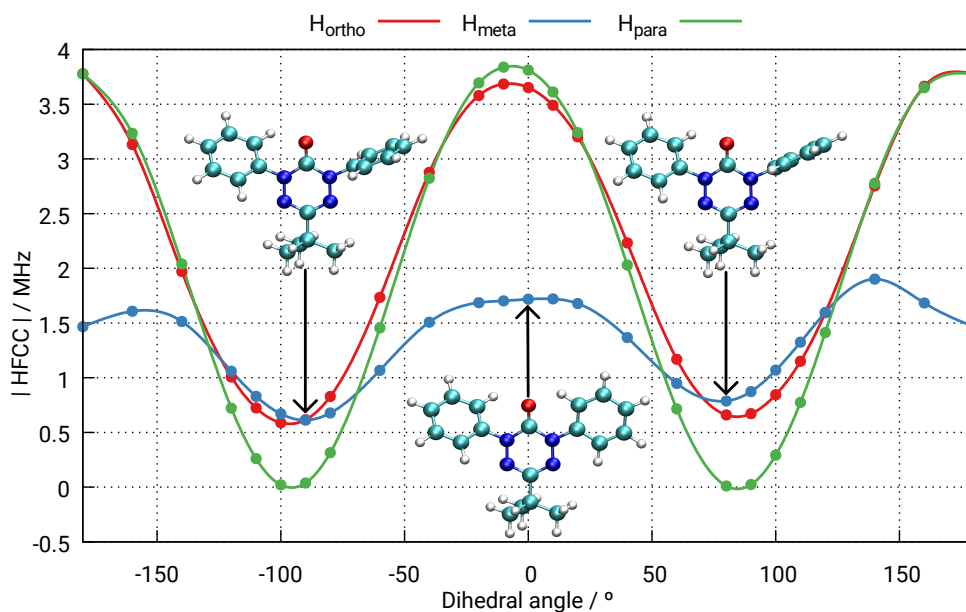
Figure S14: Dependency of the absolute HFCC value of one *ortho*, *meta* or *para* hydrogen atom located at the phenyl group on the dihedral angle of this phenyl group with respect to the verdazyl ring. The geometries which correspond to the minima and maxima of this graph are also shown.

S5 Neglecting the Hydrogen HFCCs

We demonstrate the influence of the initial guess for the line width on the fitting result when the ^{1}H HFCCs are neglected. The RMSD value was calculated via

$$\text{RMSD} = \sqrt{\frac{\sum\limits_{i=1}^{N}(y_i^{\text{exp}} - y_i^{\text{fit}})^2}{N}}, \tag{S4}$$

where y is the relative intensity at point i of the spectrum and N is the number of recorded points (see Tab. S14).

Table S4: EPR parameters and RMSD values for compound **3e**, solvated in toluene, resulting from fitting the spectrum with different inital guesses for the line width.

	Fit 1	Fit 2	Fit 3
g-shift:	0.0014	0.0014	0.0014
$A_{\text{N1,5}}$:	12.79 MHz	12.36 MHz	12.20 MHz
$A_{\text{N2,4}}$:	17.69 MHz	17.65 MHz	17.89 MHz
Gaussian lw:	0.00 MHz	0.27 MHz	0.32 MHz
Lorentzian lw:	0.47 MHz	0.24 MHz	0.12 MHz
RMSD:	0.046	0.056	0.052

Tab. S4 lists three possible fit results which were achieved by changing the initial guess of the line width. Here, the HFCCs of the hydrogen nuclei were neglected to demonstrate that their influence on the spectrum can be mimicked by a large line width. The corresponding spectra are shown in Fig. S15.
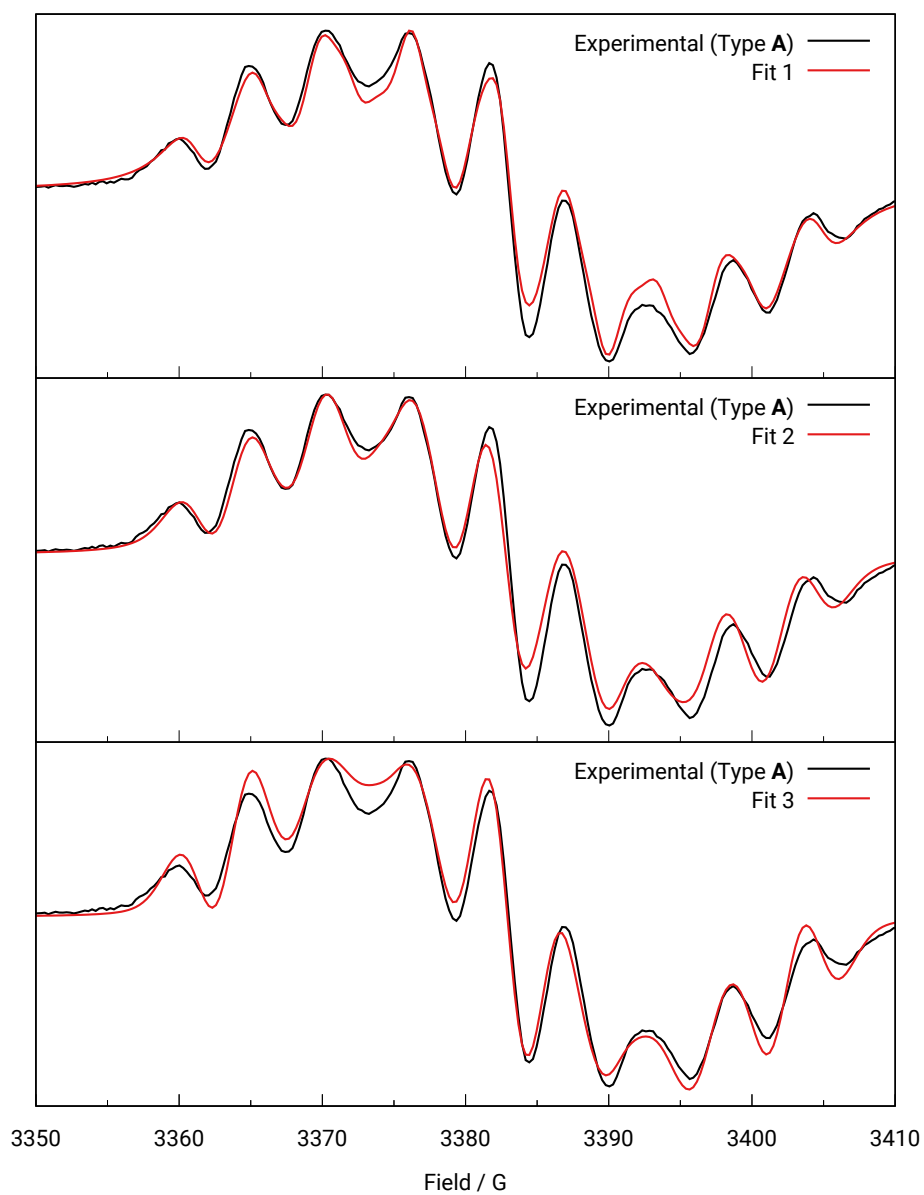
Figure S15: Spectra for compound **3e**, solvated in toluene, resulting from fitting the spectrum with different initial guesses for the line width and different ranges of freedom for the optimization of the HFCCs of the ^{14}N nuclei.

S6   Additional EPR Spectra

In the following we present additional EPR spectra, which are mentioned in the main text and illustrate the effect of various calculation details or technical settings.

S6.1   SP QM Calculated Spectra

Fig. S16 and S17 show the SP QM (type **B**) calculated spectra for all investigated compounds. It is clearly visible that the experimental and simulated spectra differ considerably.
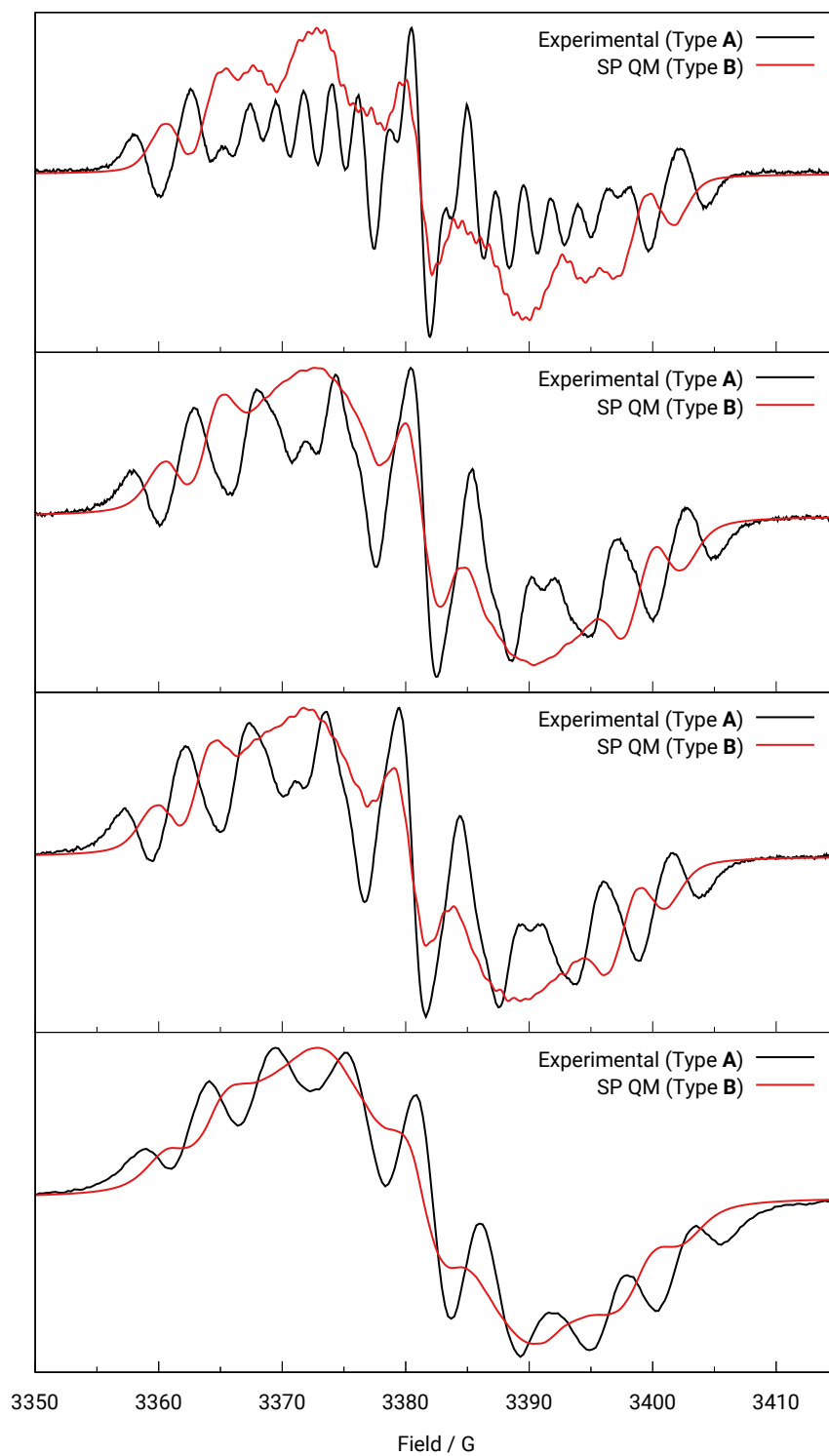
Figure S16: Experimentally measured and QM SP calculated (type **B**) spectra of compounds **3a**, **3c**, **3e** (in CH₂Cl₂) and **3g** (in toluene).
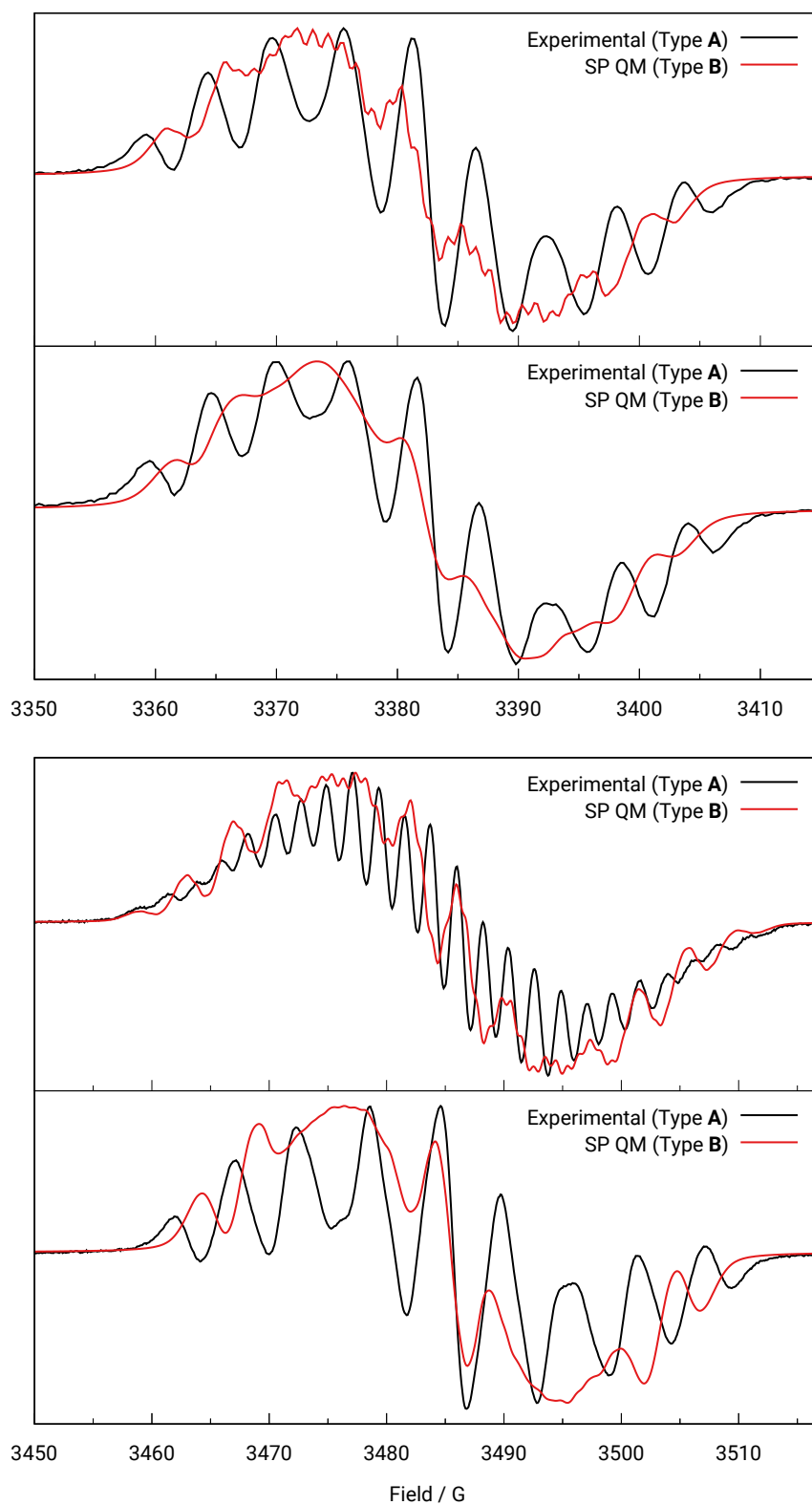
Figure S17: Experimentally measured and QM SP calculated (type **B**) spectra of compounds **3h**, **3i**, (in toluene) and **3j** and **3k** (in CH$_2$Cl$_2$).

S6.2   Influence of the Sampling Strategy

In Fig. S18 the influence of different sampling strategies on the simulated spectrum is shown.
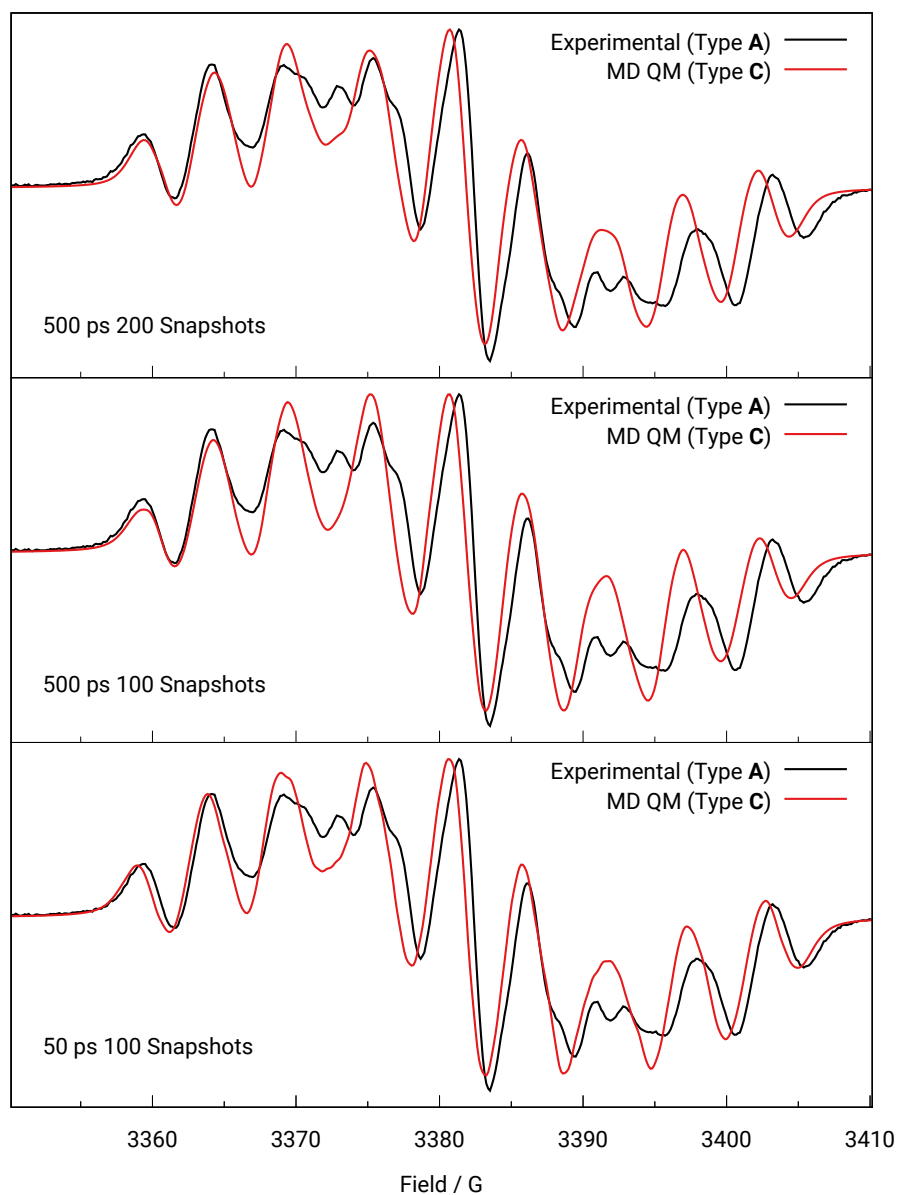
Figure S18: Comparison between simulated spectra employing different sampling strategies with the experimental EPR spectrum of system **3a** (in toluene).

S6.3 Influence of the Line Width

In this section we investigate the influence of the line width on the MD-QM calculated (type **C**) spectra by applying various different line widths on the type **C** spectrum of compound **3h**.
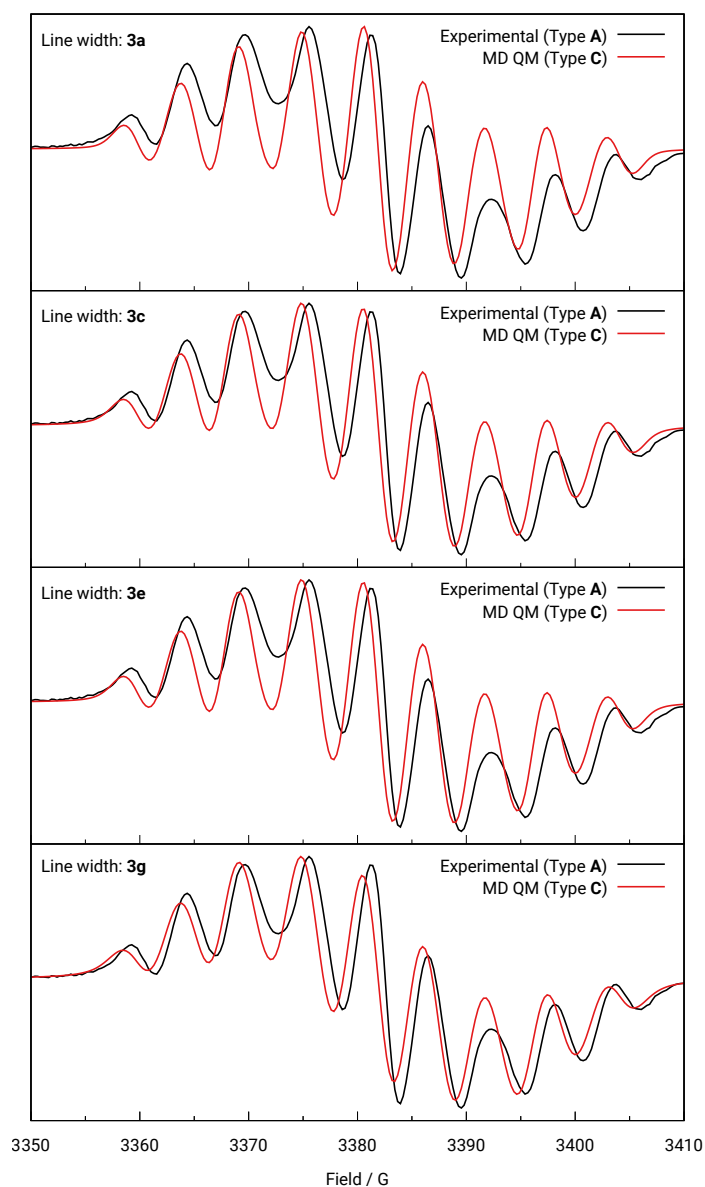
Figure S19: Experimentally measured and MD QM calculated (type **C**) spectra of compound **3h**. The line widths of compound **3a**, **3c**, **3e** (in CH$_2$Cl$_2$) and **3g** (in toluene) were used for the simulation of the spectrum of **3h**.
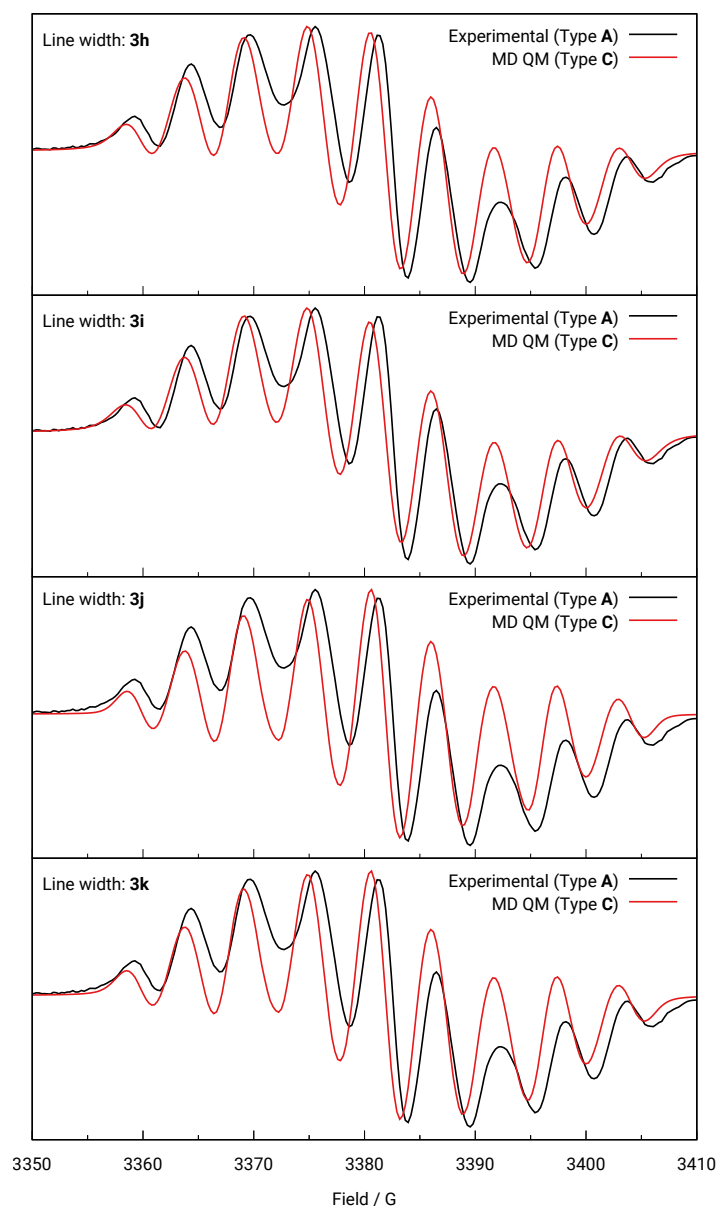
Figure S20: Experimentally measured and MD QM calculated (type **C**) spectra of compound **3h**. The line widths of compound **3h**, **3i**, (in toluene) and **3j** and **3k** in CH₂Cl₂ were used for the simulation of the spectrum of **3h**.

Slightly different intensity patterns are observed when the line widths obtained for the other investigated compounds are applied to the type **C** spectrum of **3h**. Nevertheless, a more complex spectrum (as obtained for **3a**), is never realized. Furthermore, spectra which are similar to the one of **3h**, like **3i**, could not be reproduced by applying the line width of these spectra on the type **C** spectrum of **3h**. This leads to the conclusion that the line width has a small effect on overall appearance of the spectra, but the non-resolved peak pattern which results of the smaller HFCC values (here: the hydrogen HFCCs) has a much larger influence on the shape of the spectrum. The reason is that the distribution of the HFCCs (mainly the HFCCs of the hydrogens) also leads to a peak broadening. Therefore, the apparent line width in the spectrum depends on the Gaussian and Lorentzian line width *and* the distribution of the HFCC values. The latter actually dominate in the examples shown above. From this it follows that the fitted Gaussian and Lorentzian line width do not translate directly into changes in the apparent spectrum.

S6.4 Influence of the Modulation Amplitude

The influence of different modulation amplitudes on the spectrum of **3b** is shown in Fig. S21.
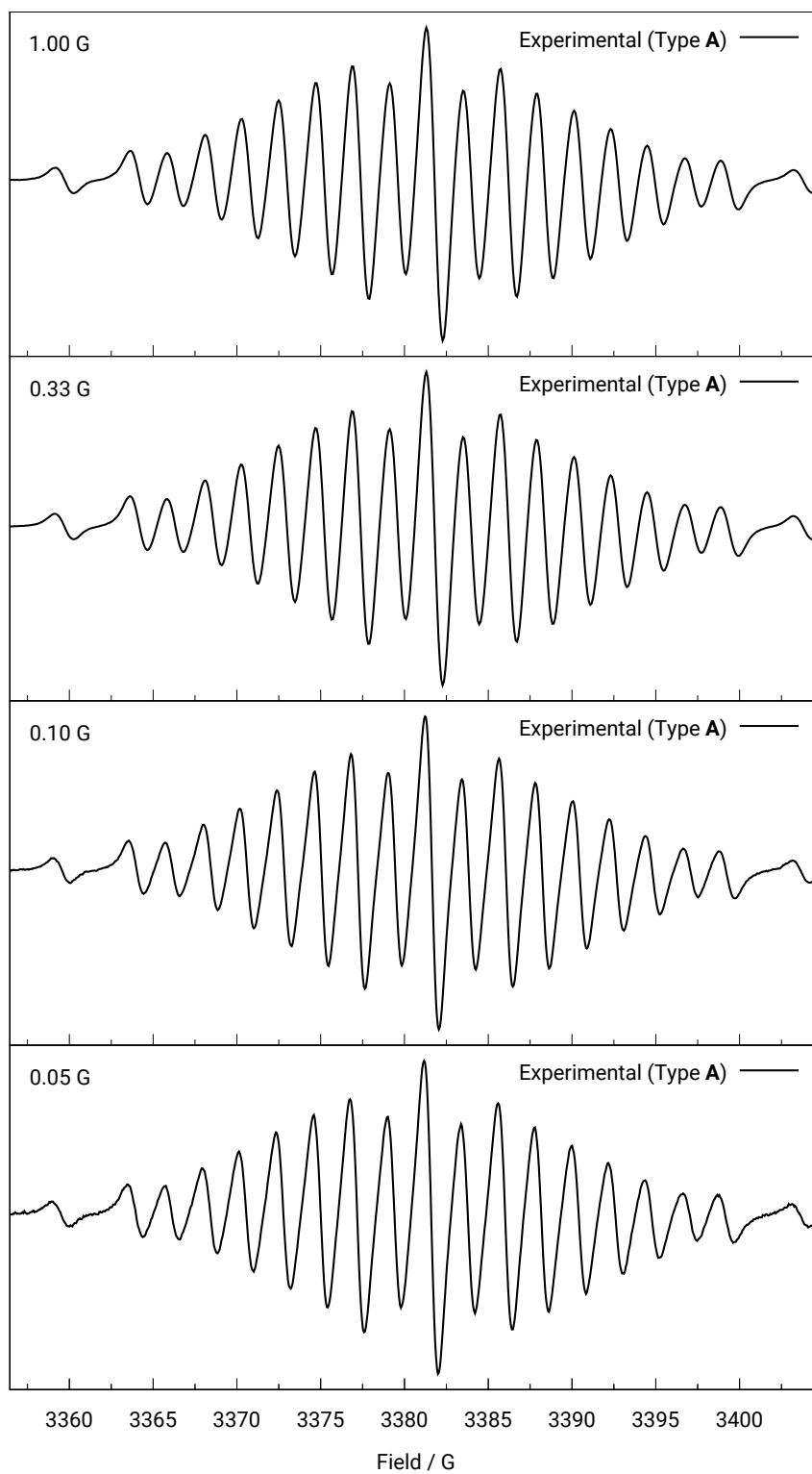
Figure S21: Experimental measured spectra of compound **3b**, solvated in CH_2Cl_2. Different modulation amplitudes were applied.

S7 EPR Parameter Comparisons

S7.1 Comparison of SP QM and MD QM Calculated EPR Parameters

Table S5: SP QM (type **B**) and MD QM (type **C**) calculated EPR parameters for all investigated compounds.

System	R		g-shift	$A_{\text{N1,5}}$ MHz	$A_{\text{N2,4}}$ MHz	$A_{\text{H, ortho}}$ MHz	$A_{\text{H, meta}}$ MHz	$A_{\text{H, para}}$ MHz
3a	*tert*-buytl	SP QM	0.0018	10.35	16.45	-2.49	1.70	-2.41
		MD QM	0.0017	13.02	17.94	-1.94	1.49	-1.71
3c	Mesityl	SP QM	0.0018	10.84	16.45	-2.45	1.72	-2.36
		MD QM	0.0017	12.10	17.56	-1.96	1.51	-1.78
3e	2-Naphthyl	SP QM	0.0018	10.63	16.18	-2.52	1.74	-2.43
		MD QM	0.0017	12.79	17.77	-2.02	1.54	-1.82
3g	1-Naphthyl	SP QM	0.0017	10.61	16.30	-2.82	1.80	-2.79
		MD QM	0.0017	12.34	17.32	-2.10	1.54	-1.97
3h	Anthracenyl	SP QM	0.0017	10.87	16.15	-2.75	1.81	-2.71
		MD QM	0.0017	13.26	17.62	-2.14	1.56	-1.94
3i	Pyrenyl	SP QM	0.0017	10.64	16.35	-2.81	1.80	-2.78
		MD QM	0.0017	12.39	17.60	-2.09	1.51	-1.91
3j[a]	Methyl	SP QM	0.0017	10.73	16.14	-2.46	1.71	-2.35
		MD QM	0.0017	12.91	17.25	-1.89	1.48	-1.66
3k	$\equiv-\text{Si}(\text{CH}_3)_3$	SP QM	0.0017	11.05	16.73	-2.48	1.74	-2.37
		MD QM	0.0017	13.22	17.83	-2.03	1.55	-1.81

[a] HFCC values of the three hydrogen atoms of the CH_3 group, which is connected to the C3 carbon, were averaged. The averaged SP QM calculated value for these ^{1}H nuclei is -10.75 MHz and the MD QM value is -10.87 MHz.

S7.2 Comparison of MD QM Calculated and Fitted EPR Parameters

Table S6: Type **C** calculated and fitted EPR parameters for compound **3a**, dissolved in CH_2Cl_2.

	MD QM values	Fitted values	Absolute difference	Relative difference
g-shift ($g^{[a]}-g_e$):	0.0017	0.0017	0.0001	4.45 %
avg. $A_{N1,5}$:	13.02 MHz	12.42 MHz	0.60 MHz	4.60 %
avg. $A_{N2,4}$:	17.94 MHz	18.47 MHz	0.53 MHz	2.97 %
$A_{H, ortho}$:	−1.94 MHz	−1.53 MHz	0.41 MHz	21.15 %
$A_{H, meta}$:	1.49 MHz	1.08 MHz	0.41 MHz	27.52 %
$A_{H, para}$:	−1.71 MHz	−1.58 MHz	0.14 MHz	7.98 %
Gaussian lw:		0.05 MHz		
Lorentzian lw:		0.11 MHz		

[a] Estimated experimental error bar: ±0.0002

Table S7: Type **C** calculated and fitted EPR parameters for compound **3c**, dissolved in CH_2Cl_2.

	MD QM values	Fitted values	Absolute difference	Relative difference
g-shift ($g^{[a]}-g_e$):	0.0017	0.0017	< 0.0001	0.79 %
avg. $A_{N1,5}$:	12.10 MHz	12.80 MHz	0.70 MHz	5.80 %
avg. $A_{N2,4}$:	17.56 MHz	18.34 MHz	0.79 MHz	4.48 %
$A_{H, ortho}$:	−1.96 MHz	−1.74 MHz	0.22 MHz	11.15 %
$A_{H, meta}$:	1.51 MHz	1.37 MHz	0.14 MHz	9.16 %
$A_{H, para}$:	−1.78 MHz	−1.69 MHz	0.09 MHz	5.11 %
Gaussian lw:		0.01 MHz		
Lorentzian lw:		0.19 MHz		

[a] Estimated experimental error bar: ±0.0002

Table S8: Type **C** calculated and fitted EPR parameters for compound **3e**, dissolved in CH_2Cl_2.

	MD QM values	Fitted values	Absolute difference	Relative difference
g-shift ($g^{[a]}-g_e$):	0.0017	0.0017	0.0001	5.00 %
avg. $A_{N1,5}$:	12.79 MHz	12.69 MHz	0.10 MHz	0.75 %
avg. $A_{N2,4}$:	17.77 MHz	18.19 MHz	0.42 MHz	2.36 %
$A_{H, ortho}$:	−2.02 MHz	−2.01 MHz	0.01 MHz	0.28 %
$A_{H, meta}$:	1.54 MHz	1.54 MHz	< 0.01 MHz	0.02 %
$A_{H, para}$:	−1.82 MHz	−1.62 MHz	0.20 MHz	11.10 %
Gaussian lw:		0.01 MHz		
Lorentzian lw:		0.17 MHz		

[a] Estimated experimental error bar: ±0.0002

Table S9: Type **C** calculated and fitted EPR parameters for compound **3g**, dissolved in toluene.

	MD QM values	Fitted values	Absolute difference	Relative difference
g-shift ($g^{[a]}-g_e$):	0.0017	0.0013	0.0004	22.02 %
avg. $A_{N1,5}$:	12.34 MHz	12.56 MHz	0.21 MHz	1.73 %
avg. $A_{N2,4}$:	17.32 MHz	18.08 MHz	0.76 MHz	4.39 %
$A_{H, ortho}$:	−2.10 MHz	−2.21 MHz	0.10 MHz	4.90 %
$A_{H, meta}$:	1.54 MHz	1.76 MHz	0.21 MHz	13.92 %
$A_{H, para}$:	−1.97 MHz	−2.01 MHz	0.05 MHz	2.45 %
Gaussian lw:		0.04 MHz		
Lorentzian lw:		0.27 MHz		

[a] Estimated experimental error bar: ±0.0002

Table S10: Type **C** calculated and fitted EPR parameters for compound **3h**, dissolved in toluene.

	MD QM values	Fitted values	Absolute difference	Relative difference
g-shift ($g^{[a]}-g_e$):	0.0017	0.0013	0.0004	23.62 %
avg. $A_{N1,5}$:	13.26 MHz	12.80 MHz	0.46 MHz	3.46 %
avg. $A_{N2,4}$:	17.62 MHz	17.93 MHz	0.31 MHz	1.74 %
$A_{H, ortho}$:	−2.14 MHz	−2.18 MHz	0.04 MHz	2.01 %
$A_{H, meta}$:	1.56 MHz	1.68 MHz	0.12 MHz	7.80 %
$A_{H, para}$:	−1.94 MHz	−1.91 MHz	0.03 MHz	1.77 %
Gaussian lw:		0.03 MHz		
Lorentzian lw:		0.19 MHz		

[a] Estimated experimental error bar: ±0.0002

Table S11: Type **C** calculated and fitted EPR parameters for compound **3i**, dissolved in toluene.

	MD QM values	Fitted values	Absolute difference		Relative difference
g-shift ($g^{[a]}-g_e$):	0.0017	0.0013	0.0004		24.54 %
avg. $A_{N1,5}$:	12.39 MHz	12.57 MHz	0.18	MHz	1.48 %
avg. $A_{N2,4}$:	17.60 MHz	18.01 MHz	0.42	MHz	2.37 %
$A_{H, ortho}$:	−2.09 MHz	−2.05 MHz	0.04	MHz	2.10 %
$A_{H, meta}$:	1.51 MHz	1.46 MHz	0.05	MHz	3.14 %
$A_{H, para}$:	−1.91 MHz	−1.75 MHz	0.16	MHz	8.34 %
Gaussian lw:		0.09 MHz			
Lorentzian lw:		0.22 MHz			

[a] Estimated experimental error bar: ±0.0002

Table S12: Type **C** calculated and fitted EPR parameters for compound **3j**, dissolved in CH_2Cl_2.

	MD QM values	Fitted values	Absolute difference		Relative difference
g-shift ($g^{[a]}-g_e$):	0.0017	0.0021	0.0003		17.87 %
avg. $A_{N1,5}$:	12.91 MHz	11.87 MHz	1.04	MHz	8.05 %
avg. $A_{N2,4}$:	17.25 MHz	16.62 MHz	0.63	MHz	3.65 %
$A_{H, ortho}$:	−1.89 MHz	−1.89 MHz	< 0.01	MHz	0.02 %
$A_{H, meta}$:	1.48 MHz	1.67 MHz	0.19	MHz	12.94 %
$A_{H, para}$:	−1.66 MHz	−1.67 MHz	0.01	MHz	0.54 %
A_{H, CH_3}:	−10.87 MHz	−6.88 MHz	3.99	MHz	36.73 %
Gaussian lw:		0.07 MHz			
Lorentzian lw:		0.07 MHz			

[a] Estimated experimental error bar: ±0.0002

Table S13: Type **C** calculated and fitted EPR parameters for compound **3k**, dissolved in CH$_2$Cl$_2$.

	MD QM values	Fitted values	Absolute difference	Relative difference
g-shift ($g^{[a]}-g_e$):	0.0017	0.0016	0.0001	6.97 %
avg. $A_{N1,5}$:	13.22 MHz	13.06 MHz	0.15 MHz	1.17 %
avg. $A_{N2,4}$:	17.83 MHz	18.24 MHz	0.41 MHz	2.31 %
$A_{H, ortho}$:	−2.03 MHz	−2.03 MHz	< 0.01 MHz	0.02 %
$A_{H, meta}$:	1.55 MHz	1.76 MHz	0.21 MHz	13.52 %
$A_{H, para}$:	−1.81 MHz	−1.79 MHz	0.02 MHz	1.09 %
Gaussian lw:		0.03 MHz		
Lorentzian lw:		0.13 MHz		

[a] Estimated experimental error bar: ±0.0002

S8   Experimental EPR Spectroscopy Data

Additional parameters used in the experiments are listed in Tab. S14.

Table S14: Modulation amplitudes, microwave power attenuation levels, microwave frequencies, sweep widths, center fields and number of recorded points used in the experimental measurements for all compounds.

System	Solvent	Modulation amplitude [G]	Microwave power attenuation level [dB]	Microwave Frequency [GHz]	Sweep width [mT]	Center field [mT]	# recorded points
3a	Toluene	0.60	29.0	9.486	13.00	331.52	1024
	CH$_2$Cl$_2$	0.30	35.0	9.484	8.00	337.99	1024
3b	CH$_2$Cl$_2$	0.05	26.0	9.483	5.65	335.25	1024
		0.10	26.0	9.483	5.65	335.25	1024
		0.33	32.0	9.483	8.27	333.94	1024
		1.00	32.0	9.483	8.27	333.94	1024
3c	Toluene	0.50	29.0	9.486	13.00	331.50	512
	CH$_2$Cl$_2$	0.50	29.0	9.485	8.00	333.99	1024
3d	CH$_2$Cl$_2$	0.03	26.0	9.483	6.00	335.07	1024
3e	Toluene	1.00	29.0	9.487	13.00	331.50	512
	CH$_2$Cl$_2$	0.40	29.0	9.482	10.00	333.10	1024
3f	CH$_2$Cl$_2$	0.10	26.0	9.482	6.00	335.07	1024
3g	Toluene	1.00	29.0	9.485	13.00	338.00	512
3h	Toluene	1.00	29.0	9.486	13.00	331.50	512
3i	Toluene	1.00	29.0	9.487	13.00	331.50	512
3j	CH$_2$Cl$_2$	0.35	32.0	9.776	9.00	344.00	1024
3k	CH$_2$Cl$_2$	1.00	32.0	9.777	9.00	344.00	1024

S9 ^{1}H- and ^{13}C-NMR spectroscopy data

2,4-Di-d$_5$-phenylcarbonohydrazide (1b)
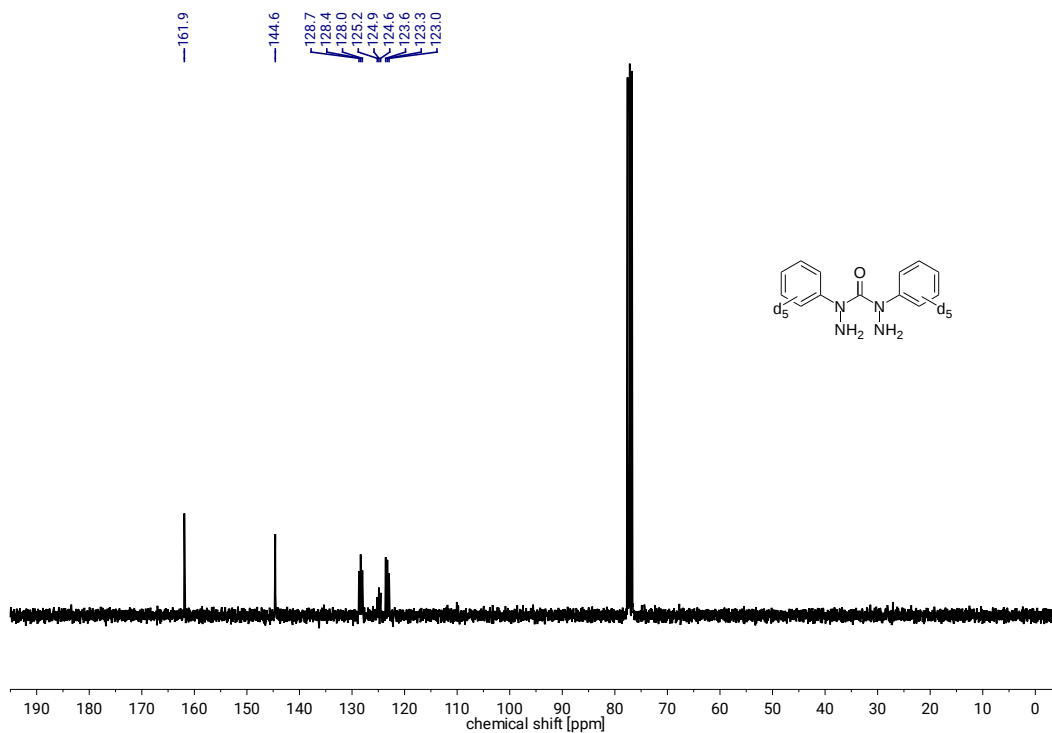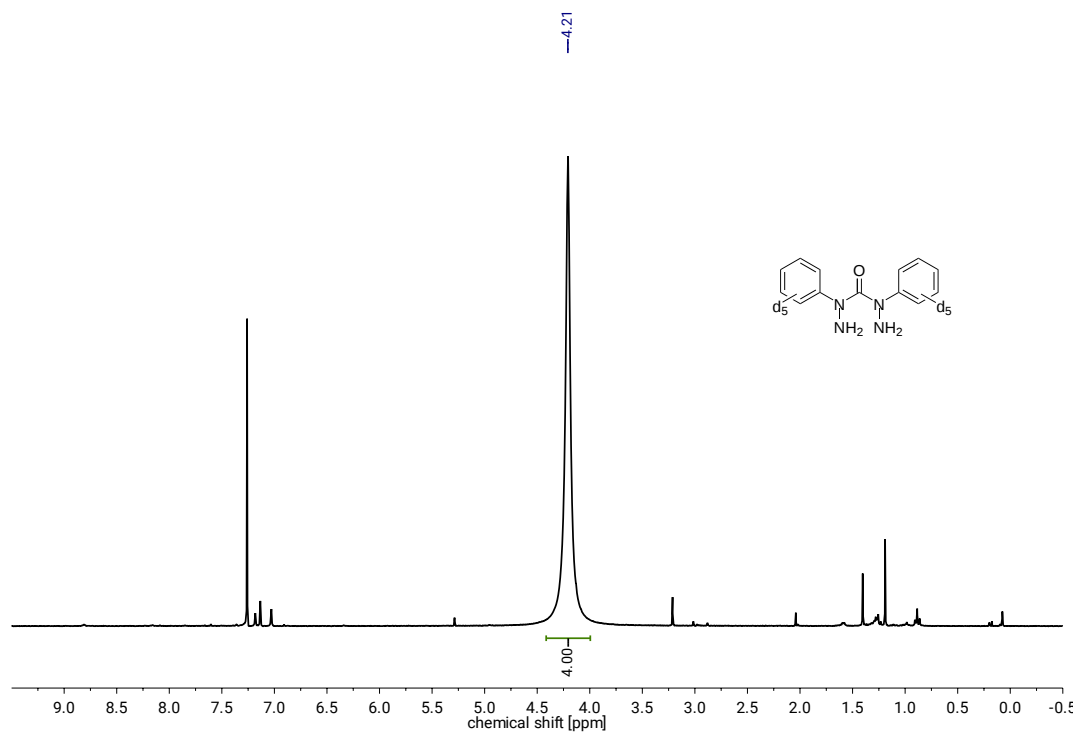
6-(Naphthalen-2-yl)-2,4-diphenyl-1,2,4,5-tetrazinan-3-one (2e)
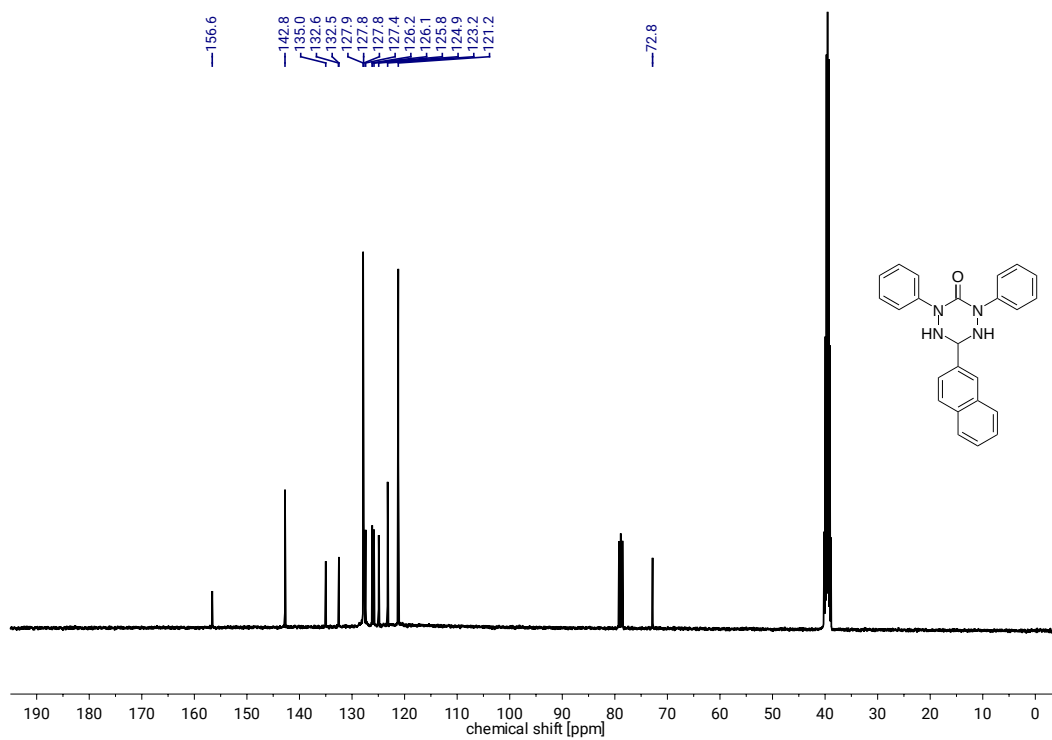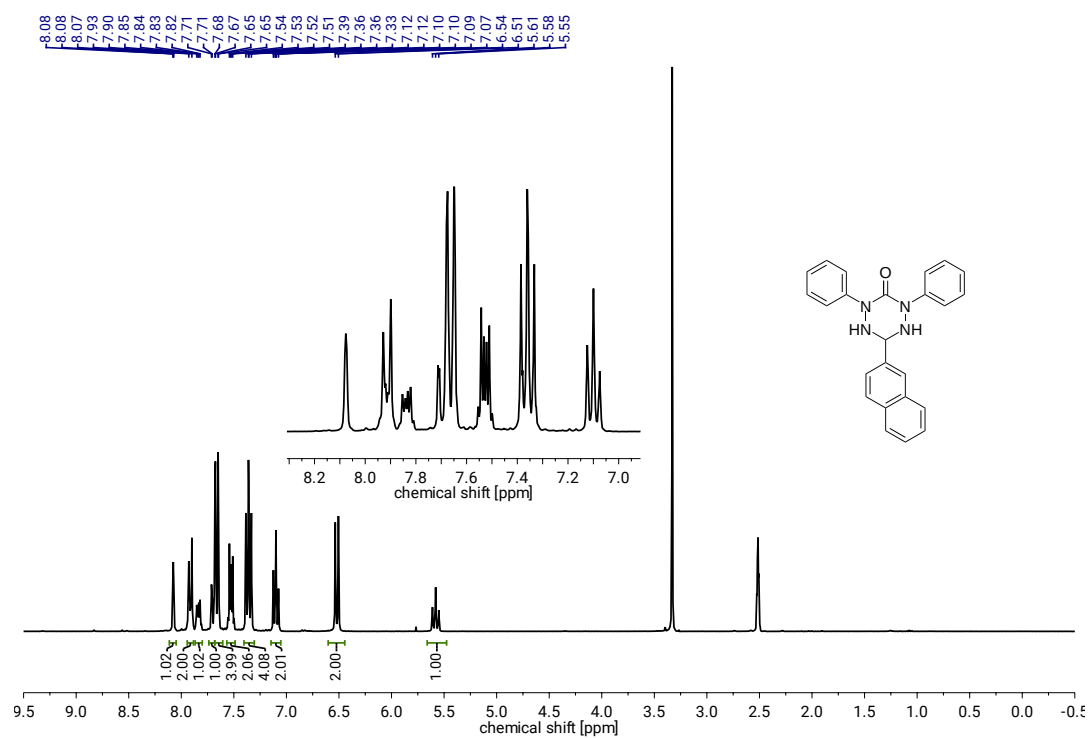
References

[1] D. Matuschek, S. Eusterwiemann, L. Stegemann, C. Doerenkamp, B. Wibbeling, C. G. Daniliuc, N. L. Doltsinis, C. A. Strassert, H. Eckert, and A. Studer, Chem. Sci. **6**, 4712 (2015).

[2] S. Eusterwiemann, D. Matuschek, L. Stegemann, S. Klabunde, C. C. Doerenkamp, C. G. Daniliuc, N. L. Doltsinis, C. A. Strassert, H. Eckert, and A. Studer, Chimia **70**, 172 (2016).

[3] D. Ghorai and J. Choudhury, Chem. Commun. **50**, 15159 (2014).

[4] Y. Masuda, M. Kuratsu, S. Suzuki, M. Kozaki, D. Shiomi, K. Sato, T. Takui, and K. Okada, Polyhedron **28**, 1950 (2009).

[5] N. Rega, M. Cossi, and V. Barone, J. Chem. Phys. **105**, 11060 (1996).

[6] M. Langgrd and J. Spanget-Larsen, J. Mol. Struct. THEOCHEM **431**, 173 (1998).

[7] G. A. A. Saracino, A. Tedeschi, G. D'Errico, R. Improta, L. Franco, M. Ruzzi, C. Corvaia, and V. Barone, J. Phys. Chem. A **106**, 10700 (2002).

[8] I. Ciofini, C. Adamo, and V. Barone, J. Chem. Phys. **121**, 6710 (2004).

[9] V. Barone, P. Cimino, and A. Pedone, Magn. Reson. Chem. **48**, S11 (2010).